PARAMETER EXTRACTION FOR BEHAVIOR MODELING OF DIODE LASERS

PARAMETER EXTRACTION FOR BEHAVIOR MODELING OF SINGLE MODE SEMICONDUCTOR LASER TRANSMITTER IN INTENSITY MODULATED DIRECT DETECTION FIBER-OPTIC COMMUNICATION SYSTEMS

BY

FAISAL HABIBULLAH , MBA, BE

A Thesis
Submitted to the School of Graduate Studies
in Partial Fulfillment of the Requirements
for the Degree
Master of Engineering

McMaster University

MASTER OF ENGINEERING (2001) McMASTER UNIVERSITY

(Electrical and Computer Engineering) Hamilton, Ontario

TITLE: Parameter Extraction for Behavior Modeling of Single Mode Semiconductor Laser Transmitter in Intensity Modulated Direct Detection Fiber-Optic Communication Systems

AUTHOR: Faisal Habibullah

B.E. (N.E.D University of Engg. and Tech. Pakistan)

MBA (Institute of Business Administration, Karachi University)

SUPERVISOR: Dr. Wei-Ping Huang

NUMBER OF PAGES: xiv, 118

Abstract

Intensity modulation direct detection (IMDD) transmission scheme has been the mainstay in optical communication ever since semiconductor lasers were put to use as the choice transmission sources. With the development of new improved laser types, this method will continue to dominate the third generation light wave networks where bit rates have steadily risen beyond 10Gbps mark. The main attraction of this scheme lies in its simplicity. With EDFA amplifiers providing a cost effective solution to the attenuation problem, long haul network capacity under the scheme has greatly increased.

At the design stage of such systems, it is essential to accurately predict the behavior of each system component right from the laser transmitter up to the optical receiver under custom specific operating conditions and laser diodes are one of the key components for a wide range of light wave communication systems. For this purpose, computer-aided simulation techniques based on behavioral models of laser diodes have been developed and validated for a variety of applications [4-8].

A 'representative' behavior model, which closely approximates the device's actual physical model, is essential to the system designer. Unfortunately, the component vendor or manufacturer may not be able to provide all the information needed to predict such behavior. The only information that can be made available, are certain measured variables over a specified measurement range. The designer therefore, needs a tool to

effectively convert this data into a useful model with sufficiently accurate parameters for predicting behavior.

As the complexity of the model increases, more detailed knowledge of the laser is required and the computation time for system performance calculation increases. While sophisticated models provide considerable insight into important characteristics of the lasers, for system simulation purposes a relatively simple model is often adequate. In this thesis we will propose a very robust and efficient procedure for estimating the modal parameters and go on to propose a complete solution to the 0D laser model extending to such domains as the below threshold dynamics and temperature effects.

Acknowledgement

I would like to sincerely thank my supervisor Dr.Wei-Ping Huang and Dr. Xun Li for their encouragement, guidance and support throughout this work. I would also like to acknowledge the help provided by Dr.Wei Li in supplying the necessary measurements from the advanced laser simulator (ALDS).

I am very much grateful to the graduate students in the Photonics Research Group for their friendship and especially to Amelia Fong and Tina Soltani for the many enlightening discussions we had, which helped me in my research.

Last of all, I am deeply ingratiated to my family especially my parents, wife and daughter for their patience and unflinching support, understanding and continued unconditional love.

Table of Contents

List of Tables

List of Figures

Chapter – 1

Introduction

The zero-dimensional rate equation model has been preferred for estimating laser system performance, in many literature, as it is independent of the structural parameters of the device (which are generally not available from the vendor) and its time-dependence makes it easy to associate and solve, with the time varying transmission signal input. A few variations and modifications of these equations have been presented. The behavioral models based on rate equations, however, require a number of modal parameters [1], which are not readily accessible to system designers. Without any doubt, the precise knowledge of these parameters is a prerequisite for the accurate prediction of the laser performance. There have been considerable development in new laser structures (e.g. DFB, DBR etc.) over the years; the basic physical interpretation however, remains the same, that the rate equations fundamentally describe the interaction between the carrier density and the photon density in the laser cavity.

1.1 Review of previous work

Efforts have long been underway to develop a behavior model, which on one hand is accurate enough to describe the device's physical behavior and at the same time, practical enough for the designer to work with for a variety of applications. The main

difficulty is that if the model is very accurate, it carries too many unknowns, making it cumbersome to handle and time consuming to solve for, likewise, if the model is simple enough to be resolved, it may overlook some key physical characteristics. We end up with solutions that would work on some devices while fail to predict the behavior of others, or on the other hand if the predicted behavior is accurate, the extraction procedure is sensitive to initial estimates or time intensive.

The two most significant achievements in this direction are by J.Cartledge etal.[1] and L.Bjerkan etal. [2] who have used contrasting techniques for estimating rate equation parameters and then using these parameters to estimate the behavior. Both authors have used the steady state *L-I* characteristics and the small signal AM-frequency response data to estimate the parameter values, in their formulations.

In the first case, an all-numerical solution is presented to solve for the nine rate-equation parameters with the obvious sensitivity problem for convergence, to the range of initial estimates made. The main advantage is that all parameters are self-consistently extracted from the same source (i.e. laser). In the latter case [2], the authors have presented a modified rate-equation model by combining various parameters and treating them as lumped unknowns. The techniques for estimating these parameters is part analytical, part numerical. Although, the method is simple and has reduced the total number of parameters to be extracted, at the same time, the data requirement needed to determine the complete set has increased, some of which is not available for most commercial lasers, most significantly, the below threshold experimental data of the *LI*-response, to compute spontaneous emission coupling parameter. Secondly, signal dispersion from a coupled fiber or laser spectral measurements were used in the process with considerable difference in the extracted parameter values computed from either source. This raises questions about the self-consistency of the data, as fiber being a different medium than laser, while the optical spectral measurements were not consistent with theoretical measurements, for all the tested devices.

1.2 Scope of this report

This work closely follows the work done in [2], with a few critical exceptions. We hope to present a workable model not only for the above threshold operating conditions but also provide for lasers, pre-biased below threshold, something, which the previous methods have not attempted. This is an important objective, owing to the fact that high temperature sensitivity of many lasers prevents them from being operated too close to or above threshold and turn-on delay assumes significance for such devices when gain-switching schemes are implemented. Secondly, in order to maintain self-consistency in the data we would utilize only measurements from the model laser itself, which would include the steady state and small signal response measurements alone. Large signal measurements are used only as a means of comparison and optimization (if required). We would also present parameter estimation techniques, which are uniquely analytical. A modified rate-equation model is presented which is different from the one used in [2].

1.3 Thesis Overview

We start off with the description of the physical dynamics that are responsible for semiconductor laser behavior under various levels of current injection. Chapter-2 details these underlying phenomenon and then goes on to develop the universal rate-equation model based on the physical model.

Chapter-3 deals with the steady state solution of the rate-equation model and draws on a few results for the most frequented, above-threshold operating conditions, based on some reasonable assumptions from the physical model. The second part of this chapter then uses these steady state solutions to modify the rate-equation model into a

form suitable for the extraction of unknown parameters or a combination of parameters. This 'Modified' rate-equation model forms the backbone of our solver. A discussion on incorporating dynamic thermal behavior from steady state temperature related changes is included as a prelude for future work.

In Chapter-4, we continue on to solve the universal rate-equations under the small signal regime and develop the relationship for small signal IM frequency transfer function, which is key to the estimation of parameters. We then formulate analytical expressions for the parameters in our modified rate-equation model that are directly extracted from the laser small signal response and steady state solution.

Chapter-5 deals with the process of verification of our extraction method by testing the model with the laser data from [1] and the simulated results of the ALDS simulator both with vastly different response characteristics. It also tests the robustness of the method by introducing a degree of variation in the parameter values and observes the effect on the simulation results.

We finally conclude with the presentation of some key results drawn from our work and the limitations and benefits of using this technique as compared to those presented in [1] and [2]. This section will also provide an outline for future research in this direction.

Chapter - 2

Laser Rate Equations – Governing physical phenomenon of a dynamic response model

2.1 Laser Diodes – Spectrally refined light sources

Laser diodes are small and coherent optical radiation sources of high intensity which can be modulated directly at high speed. In fiber optics communication systems a number of additional requirements need to be met such as

- Spectral characteristics matching the fiber characteristics
- Continuous operation up to the temperatures occurring in the transmitter and at specified optical output powers (typically 5 to 10mW)
- Stability in spatial and spectral distribution of the laser emission
- Adequate stability of the principal laser characteristics over long periods of operation
- A sufficiently simple, i.e. economical fabrication method.

An important measure in fulfilling these requirements is the internal structuring of the laser in addition to the external confinement by the two mirror surfaces. This serves to confine the electrically pumped region around the p-n junction and the optical cavity to a small region in the laser crystal. An essential pre-requisite for continuous operation at and

above room temperature is the vertical confinement of the charge carriers and the optical wave by the '*double hetrostructure*' to an active region usually only 0.1 to 0.2 μm thick.

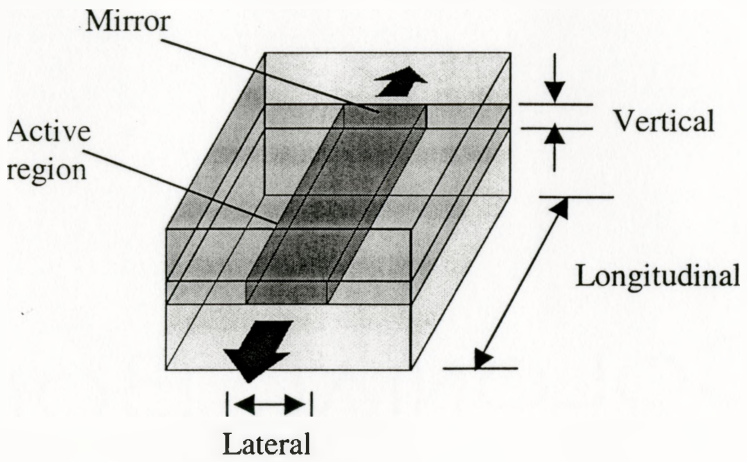

Fig.2.1 Spatial confinement of the active region of a laser diode

An important factor as regards the optical stability of the laser diodes is the lateral confinement. This compels the laser to oscillate (nearly) in the fundamental mode only and prevents higher-order modes from propagating. This prevents such instabilities as kinks in the characteristics, large emission noise and the possibility of the far field fluctuating as a result of competing modes. It also prevents deformation of the lateral gain profile by the stimulated emission itself.

2.2 The physical model

If we consider the laser as a light source, then we need to establish the fact that to maintain continuous generation of light (photons), the laser needs a gain medium and

some sort of feedback (like an RF oscillator). The gain is provided by the active material laser cavity and the facet reflection provides the necessary feedback.

Without going into details of the material properties or the band-gap structure of laser cavity, it is suffice to say that in the double hetrostructure of a semiconductor laser (e.g. N-p-P), under certain condition of forward bias, free electrons are injected into the cavity from both sides. The thermal equilibrium of the free electrons is disturbed and more electrons are pumped from the valence band into the conduction band, making the conduction band as a reservoir of free electrons (and simultaneously making the valence band a reservoir of holes). The capacity of this reservoir increases in direct proportionality to the increasing injection level.

The fermi-levels, which define the probability of occurrence of both electrons and holes (and in turn the band-gap energy level) within the band structure, are therefore shifted from their equilibrium position into the respective valence and/or conduction bands. The high-energy electrons in the conduction band can undergo several phenomenons.

a. Some recombine with the holes through *non-radiative* (indirect) recombination, such that the energy released in the form of photons is less than the band-gap energy and is absorbed without causing any excitement.

b. Others recombine spontaneously (direct transition from conduction to valence band) the energy released is equal to or higher than the band-gap energy and can excite further electrons from valence into conduction band. At low injection levels, only a fraction of these *spontaneous recombinations* emit photons into the mode of interest and the released energy leaves the cavity to contributes to the laser output.

c. As the injection level is gradually increased, so does the spontaneous recombination, which excites more electrons into the conduction band, giving rise to the phenomenon called *stimulated absorption*. Stimulated absorption events create new carriers and are also responsible for the disappearance of photons.

d. At sufficiently high levels of injection, these electrons can recombine with the valence band holes and in the process release photons having twice the energy with the same direction and phase as the absorbed photon energy. Thus, at this stage energy amplification takes place and the phenomenon is called *stimulated emission.* Stimulated emission events provide a recombination path for the carriers and are the source of new photons.

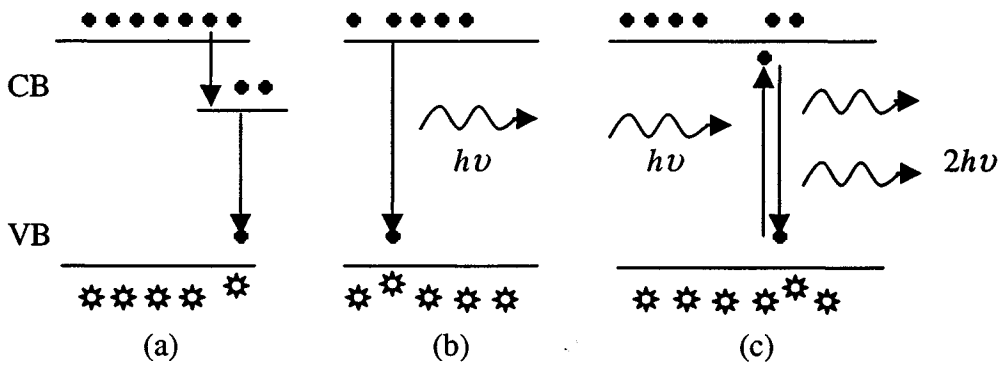

Fig.2.2 Electron transitions between conduction and valence bands and the generation of photons. (a) Non-radiative recombination; (b) Spontaneous emission (c) Stimulated absorption and emission.

Once stimulated emission is obtained, the gain inside the cavity balances the losses (due to absorption from non-radiative recombination mirror reflectivity) and the laser is said to have achieved its threshold. Any further increase in the injected current

directly contributes to the laser light output depending upon the output coupling efficiency.

The dynamic response of semiconductor laser can be quite accurately predicted, if we can obtain the time response of the photon density in the active region of the laser cavity in response to the electrical excitation current injected into the device.

2.3 Developing the rate equation model

Now let us formulate the time dependence of carrier and photon densities inside the cavity with the underlying assumption that all perturbations within the cavity are uniform everywhere, or, in other words there is no spatial dependence associated with the carriers and photons.

When a laser is subjected to a positive voltage across the terminals, current flows in and carriers accumulate around the junction of the cavity. In practice, a fraction of the injected current reaches the cavity and the leakage carriers are defined by the '*internal quantum efficiency*' (η_i). For the DH active region, the rate of change in carrier density is

$$\frac{dN}{dt} = G_g - R_r$$

The injected current provides the generation term above (G_g), while the various recombination processes (as well as carrier leakage) which reduces the carrier density in the conduction band, contribute to the recombination term (R_r). A portion of the injected $\frac{J}{q}$ carriers cross the interface and are confined within a narrow width 'd' of the cavity.

Thus the rate of injection is given by

$$G_g \propto \frac{J}{qd} \qquad \text{Or} \qquad G_g \propto \frac{I}{qV}$$

$$G_g = \eta_i \frac{I}{qV}$$

Where 'V' is the volume of the active region. The recombination process must encompass all the possible mechanisms discussed earlier. Therefore, combining spontaneous emission rate, non-radiative recombination rate and the stimulated emission rate

$$R_r = R_{sp} + R_{nr} + R_{st}$$

Where

$$R_{st} = R_{st(emission)} - R_{st(absorption)}$$

We have neglected the leakage term in the above relation assuming that the lateral and/or transverse potential barriers are sufficiently high. The first two terms describes the natural decay process of carriers within the cavity, which is governed by the spontaneous emission '*carrier lifetime*' (τ_N)

The stimulated recombination term requires the presence of photons inside the cavity. In the absence of photons the carrier rate equation is simply the sum of spontaneous recombination and the non-radiative recombination rates

$$\frac{dN}{dt} = \frac{N}{\tau_N} = R_{sp} + R_{nr}$$

Given that

$$N = n_0 e^{-\frac{t}{\tau_N}}$$

Where n_0 is the original carrier density before injection. Since each term on the RHS depends upon the existence of carriers, the natural decay of carriers can actually be expressed as a power series expansion of the carrier density.

$$R_r = \frac{N}{\tau_N} = BN^2 + \left(AN + CN^3\right)$$

Where 'B' is the bimolecular recombination coefficient and defines the spontaneous recombination rate. Our carrier rate equation now becomes

$$\frac{dN}{dt} = \eta_i \frac{I}{qV} - R_{st} - \frac{N}{\tau_N}$$

R_{st} represents the photon-stimulated net electron-hole recombination, which generates more photons. This is thus a <u>*gain*</u> process for photons facilitated by the injected current. As illustrated in the figure, the net effect of the upward and downward electronic transitions, corresponding to the stimulated absorption and emission of photons, respectively, is shown to be a <u>*growth*</u> of photon density from an initial (or incoming) value of 'S_i' to an outgoing value of 'S_o' with increment 'ΔS', as it passes through a small length 'ΔL' of the gain medium (active region or laser cavity).

$$S_o = S_i + \Delta S$$

Let 'g' be the gain per unit length inside the cavity. The cavity volume occupied by the photons is much larger than the active region volume occupied by the electrons and there is a partial overlap between the active region and the photon field (which is true in practice) defined by the '*gain confinement factor*' (Γ).

We can also describe this photon growth as

$$S_i + \Delta S = S \exp(\Gamma g \Delta L)$$

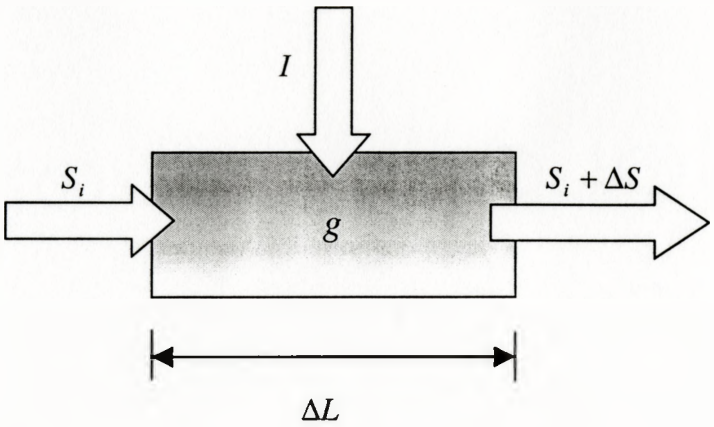

Fig 2.3 The simplified laser cavity gain model

If 'v_g' is the group velocity of photons,

$$\Delta L = v_g \Delta t$$

If the cavity length is sufficiently small, then we can make the following approximations.

$$\exp(\Gamma g \Delta L) \approx 1 + \Gamma g \Delta L$$

Thus,

$$\Delta S = \Gamma g \Delta L S = \Gamma g v_g \Delta t S$$

And

$$\left.\frac{dS}{dt}\right|_{st-gen} = \Gamma g v_g S$$

Photon generation from spontaneous emission is random and the contribution is assumed equally likely for all possible optical modes within the laser cavity. This implies that a small portion of these spontaneously emitted photons are in phase with the mode of interest and contribute to the gain. This contribution from spontaneous emission is

$$\left.\frac{dS}{dt}\right|_{sp-gen.} = \Gamma\beta R_{sp} = \Gamma\beta\frac{N}{\tau_N}$$

Where, we define 'β' as the factor that determines the fraction of spontaneous emission photons into the lasing mode.

Photon loss occurs within the cavity due to optical absorption and scattering out of the mode, and it also occurs at the output-coupling mirror where a portion of the useful mode is usually coupled to some medium (such as fiber). We can characterize the net loss by a *photon (cavity) lifetime* 'τ_P'. Analogous to the carrier decay, the photon lifetime defines the photon decay and is quantified by.

$$\frac{1}{\tau_P} = \frac{1}{\tau_i} + \frac{1}{\tau_m} = v_g(\alpha_i + \alpha_m)$$

Where 'α_i' and 'α_m' characterize the internal cavity loss and mirror loss respectively.

Thus, the net loss of photons from the cavity, is given by

$$\left.\frac{dS}{dt}\right|_{loss} = \frac{S}{\tau_P}$$

We can now formulate our photon rate equation.

$$\frac{dS}{dt} = \Gamma v_g gS - \frac{S}{\tau_P} + \Gamma\beta\frac{N}{\tau_N}$$

The stimulated emission term in the carrier rate equation can now be defined as

$$R_{st} = v_g gS$$

Note that the gain confinement factor is not included since the electrons lie within the active region and there is no need to account for an overlapping field as in the case of photons. The carrier rate equation is thus given by

$$\frac{dN}{dt} = \eta_i \frac{I}{qV} - v_g gS - \frac{N}{\tau_N}$$

For the purpose of behavior modeling the internal quantum efficiency is generally neglected, as it does not affect the overall response function of the laser. Therefore,

$$\frac{dN}{dt} = \frac{I}{qV} - v_g gS - \frac{N}{\tau_N}$$

Now, as the carrier density increases with increasing injection level, the gain in the cavity increases, however, the laser will not be able to sustain a stimulated emission of photons unless this gain overcomes all the cavity losses including mirror losses.

If we consider the excess electrons in the conduction band as a source of photons inside the cavity, then it will be easy to understand that a sufficient level of electron buildup is required before we have positive gain inside the cavity. This minimum level is called the '*transparency level*'. Thus, when the carrier injection is high enough to create a quasi-Fermi level separation exceeding the band gap, we have positive gain.

$$E_g < h\upsilon < \Delta E_f$$

The rate of increase in gain with increasing carrier density is characterized by '*differential gain*'. For all practical purposes this is assumed to be a constant device parameter, however, more realistically it decreases on a logarithmic scale. Total cavity gain as a function of carrier density can now be approximated as a straight line

$$g|_{total} = v_g g \approx \frac{\partial g}{\partial N}(N - N_T)$$

The total gain variation (dg) can be explained by assuming it is affected by both carrier and photon density, such that

$$dg = adN - a_p dS$$

This indicates that gain is directly proportional to an increase in carrier density while it decreases with an increase in photon density. In terms of total gain this inverse proportionality to photon density is expressed as

$$g(N,S) \propto \frac{1}{1+\varepsilon S}$$

$$g(N,S) = \frac{g_0}{1+\varepsilon S}(N - N_T)$$

From which we can obtain

$$\frac{dg}{dN} \approx \frac{\partial g}{\partial N} = \frac{g_0}{1+\varepsilon S}$$

For simplicity, we have neglected the differential gain component due to variation in photon density, since this component is very small. Our model is a behavior model, which will generally work in the linear region of the laser operation above threshold.

Thus the partial derivative of gain with respect to carrier density represents the total gain variation for all practical purposes. The universal 0D coupled rate equation model for single operating mode, can now be completely represented as follows

$$\frac{dS}{dt} = \frac{\Gamma g_0 (N - N_T) S}{1 + \varepsilon S} - \frac{S}{\tau_P} + \Gamma \beta \frac{N}{\tau_N} \tag{2.1}$$

$$\frac{dN}{dt} = \frac{I}{qV} - \frac{g_0 (N - N_T) S}{1 + \varepsilon S} - \frac{N}{\tau_N} \tag{2.2}$$

The parameters that define the intrinsic properties of the laser in this model are listed in table 2.1.

Description	Symbol	Unit
Active region volume	V	cm^3
Gain confinement factor	Γ	au
Gain slope constant	g_0	cm^3 / s
Differential quantum efficiency	η_D	au
Average photon lifetime	τ_P	s
Carrier lifetime	τ_N	s
Transparency carrier density	N_T	cm^{-3}
Gain compression factor	ε	cm^3
Spontaneous emission factor	β	au

Table 2.1

The parameters represent various structural characteristics of the laser cavity and in turn are reflected in the device performance curves to varying inputs. It is very difficult to uniquely determine all these parameters as have been evident in the previous works [1],[2]. We will however, try to isolate some of these parameters and for those which cannot be isolated, a lumped parameter will be estimated from the performance characteristics of the device alone.

2.4 Representation of refractive index modulation effect

Current modulation of the active region results in the modulation of both the photon density and the carrier density. The modulation of the carrier density modulates the gain, however, it also modulates the index of the active region (n_a). This is equivalent to altering the length of the cavity and as a consequence, the resonant mode shifts back and forth in the frequency. This frequency modulation (FM) is desirable only if we want to dynamically tune the laser, but for intensity modulation (IMDD) applications, this phenomenon is undesirable noise at the output of modulated light spectrum as it broadens the linewidth.

The optical energy of a diode laser propagates in a dielectric wave-guide mode, which is confined both transversely and laterally, defined by a normalized transverse electric field profile $U(x,y)$. In the axial direction this mode propagation can be represented by a time-space varying electric field

$$\vec{E} = \hat{e}\,|E_0|U(x,y)e^{j(\omega t-\tilde{\beta}z)} \qquad (2.3)$$

The complex propagation constant $\tilde{\beta}$ includes the incremental transverse modal gain and incremental modal loss terms found from the weighted averages of the gain and loss.

$$\tilde{\beta} = \beta + j\beta_i = \beta + \frac{j}{2}\left(\langle g \rangle_{xy} - \langle \alpha_i \rangle_{xy}\right)$$

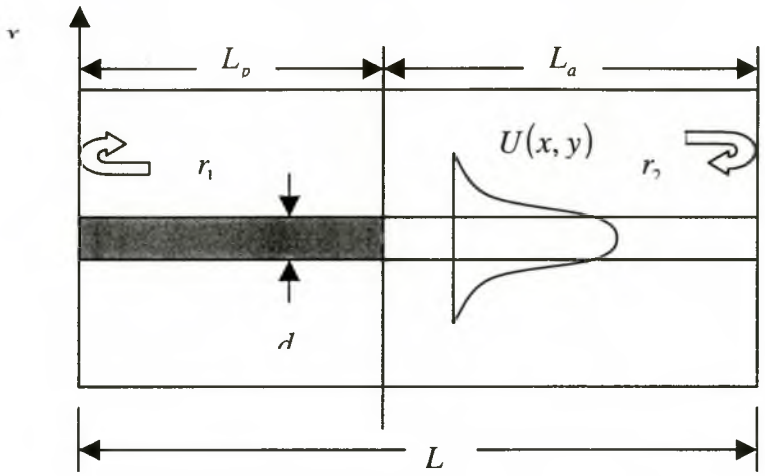

Fig.2.4 Laser cavity with active and passive regions together with the mode profile

The real part of the propagation constant is given by

$$\beta = \frac{2\pi\bar{n}}{\lambda} \tag{2.4}$$

Most laser cavities can be divided into two general sections: an active section of length L_a and a passive section of length L_p with zero gain (figure-2.4). The propagating mode is reflected by end mirrors with amplitude reflection coefficients r_1 and r_2 respectively, to provide a resonant cavity.

In order for the gain in the active region to reach threshold, the gain in the active section must be increased to a level where all the mirror and cavity losses are

compensated and the electric field exactly compensates itself after one round trip in the cavity.

$$E(z = 2L) = E(z = 0)$$

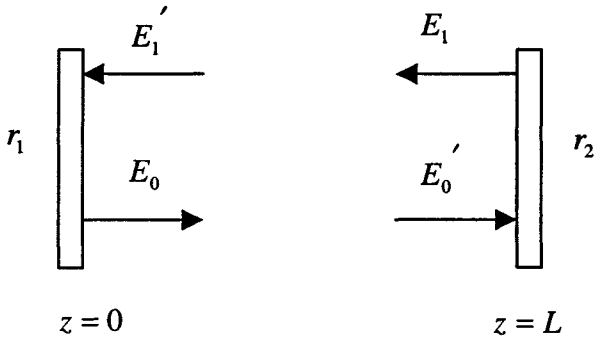

Fig.2.5. A schematic of the cavity representing the boundary condition for threshold

By introducing the mode reflection coefficients at the two boundaries we implement the boundary condition for threshold.

$$E_0' = E_0 e^{(g-\alpha)L}$$

$$E_1' = r_1 E_0 e^{2(g-\alpha)L}$$

$$\therefore E_0 = r_1 r_2 E_0 e^{2(g-\alpha)L}$$

And

$$r_1 r_2 e^{2(g-\alpha)L} = 1$$

In the case of a 2-section cavity, this can be represented as

$$r_1 r_2 \exp\left(-2j\tilde{\beta}_{ath} L_a\right)\exp\left(-2j\tilde{\beta}_{pth} L_p\right) = 1$$

For this equation to be valid, the real part of the propagation constant must be equated as

$$\beta_{ath} L_a + \beta_{pth} L_p = m\pi$$

Making substitution from equation (1.4) above

$$\lambda_{th} = \frac{2}{m}\left[\bar{n}_a L_a + \bar{n}_p L_p\right]$$

Or

$$\upsilon\left[\bar{n}_a L_a + \bar{n}_p L_p\right] = \frac{mc}{2} \qquad (2.5)$$

In this relation, the refractive index is a function of both wavelength and carrier density, thus the effect of variation of both has to be accounted. If we have the two variables as

$$N = N_0 + \Delta N \quad \text{and} \quad \lambda = \lambda_0 + \Delta\lambda$$

Then

$$\bar{n}(\lambda, N) = \bar{n}(\lambda_0, N_0) + \frac{\partial \bar{n}}{\partial \lambda}\Delta\lambda + \frac{\partial \bar{n}}{\partial N}\Delta N$$

If we take the differential of equation (2.5) and include the above variations, then the first term of this differential is given by

$$\Delta(\upsilon\bar{n}_a) = \Delta\upsilon\bar{n}_a + \upsilon\left[\frac{d\bar{n}_a}{d\upsilon}\Delta\upsilon + \frac{d\bar{n}_a}{dN}\Delta N\right]$$

If we define the group refractive index as

$$\bar{n}_g \equiv \bar{n} + \upsilon \frac{d\bar{n}}{d\upsilon}$$

Then

$$\Delta(\upsilon \bar{n}_a) = \Delta \upsilon \bar{n}_{ga} + \upsilon \frac{d\bar{n}_a}{dN} \Delta N$$

For the passive section

$$\Delta(\upsilon \bar{n}_p) = \Delta \upsilon \bar{n}_{gp}$$

Equating the original differential equation to zero

$$\Delta \upsilon \bar{n}_{ga} L_a + \Delta \upsilon \bar{n}_{gp} L_p + \upsilon \bar{n}_{ga} L_a \frac{d\bar{n}_a}{dN} \Delta N = 0$$

$$\Delta \upsilon = -\frac{\upsilon \bar{n}_{ga} L_a}{\bar{n}_{ga} L_a + \bar{n}_{gp} L_p} \frac{d\bar{n}_a}{dN} \Delta N$$

Defining the transverse gain confinement factor for the active cavity as

$$\Gamma_z \equiv \frac{\bar{n}_{ga} L_a}{\bar{n}_{ga} L_a + \bar{n}_{gp} L_p}$$

We get

$$\Delta \upsilon = -\Gamma_z \upsilon \frac{d\bar{n}_a}{dN} \Delta N$$

$$\Delta \upsilon = -\Gamma_z \frac{v_g}{\lambda} \frac{d\bar{n}_a}{dN} \Delta N \qquad (2.6)$$

Where v_g is the group velocity.

The change in effective propagation index can be related to the change in active material index through the relation

$$\Delta\bar{n} = \Gamma_{xy}\Delta n$$

$$\frac{d\bar{n}}{dN} = \Gamma_{xy}\frac{dn}{dN}$$

Making this substitution in equation (2.6)

$$\Delta\upsilon = -\Gamma_z\Gamma_{xy}\frac{v_g}{\lambda}\frac{dn_a}{dN}\Delta N$$

$$\Delta\upsilon = -\frac{\Gamma v_g}{\lambda}\frac{dn_a}{dN}\Delta N \qquad (2.7)$$

From our previous discussion of mode propagation inside a cavity, we know that the imaginary part of the propagation constant is proportional to the cavity gain.

$$g = 2\beta_0 n_i = \frac{4\pi n_i}{\lambda}$$

Where n_i is the imaginary part of the refractive index.

$$\frac{dg}{dN} = \frac{4\pi}{\lambda}\frac{dn_i}{dN}$$

We now define the *'linewidth enhancement factor'* as the ratio of the rate of change of real and imaginary refractive indices with respect to a change in carrier density.

$$\alpha \equiv -\frac{dn/dN}{dn_i/dn} = -\frac{4\pi}{\lambda}\frac{dn/dN}{dg/dN}$$

Replacing $\frac{dn_a}{dN}$ in equation (2.7) with the above, we get the frequency shift in response to changes in carrier density

$$\Delta\upsilon = \frac{\alpha}{4\pi}\Gamma v_g \frac{dg}{dN}\Delta N$$

$$\Delta\upsilon = \frac{\alpha}{4\pi}\Gamma v_g a\Delta N \tag{2.8}$$

Where a is the differential gain coefficient.

Now taking the photon density rate equation we solve for the difference between gain and loss terms.

$$\Gamma v_g g - \frac{1}{\tau_P} = \frac{1}{S}\frac{dS}{dt} - \Gamma\beta\frac{N}{S\tau_N}$$

The carrier density and gain are clamped at threshold and we can approximate this gain around threshold.

$$g = g_{th} + a(N - N_{th})$$

Where we have neglected the gain component due to the photon density as photon density is still very small around threshold.

$$\therefore \Gamma v_g g_{th} + \Gamma v_g a(N - N_{th}) - \frac{1}{\tau_P} = \frac{1}{S}\frac{dS}{dt} - \Gamma\beta\frac{N}{S\tau_N}$$

We can neglect the spontaneous emission term above threshold, on the RHS of the equation, and can approximate the first term as

$$\Gamma v_g g_{th} \approx \frac{1}{\tau_P}$$

Therefore

$$\Gamma v_g a(N - N_{th}) \approx \frac{1}{S}\frac{dS}{dt}$$

From equation (2.8), we can now define the frequency shift in terms of the photon density, using the above relation

$$\Delta \upsilon = \frac{\alpha}{4\pi}\left[\frac{1}{S}\frac{dS}{dt}\right]$$

Or

$$\Delta \upsilon = \frac{\alpha}{4\pi}\left[\frac{1}{P}\frac{dP}{dt}\right] \qquad [\text{Since } S \propto P]$$

We can directly compute the phase rate equation from equation (2.8)

$$2\pi\Delta\upsilon = \alpha\frac{1}{2}\Gamma g_0(N - N_{th})$$

$$\frac{d\phi}{dt} = \alpha\frac{1}{2}\Gamma g_0(N - N_{th}) \qquad (2.9)$$

Once the linewidth enhancement factor is known the phase rate equation can be used to compute the laser's dynamic frequency chirp at different bias levels subject to the injected current. This provides a useful insight into the spectral stability of the device and limitation for the modulation frequency.

Chapter-3

'Modified' Rate Equations and a Simplified model for Temperature Induced Behavior

3.1 Steady state solution of the rate equations

The solutions of the rate equations for DC excitation are well documented. This section will outline few of the results of this solution together with developing a functional relationship of the steady state photon density with the DC bias current, through an analytical expression.

Under steady state conditions, the rate of change in carrier and photon densities is zero and we can apply this simplification to our rate equation models, given that

$$\frac{dN}{dt} = 0, \qquad N \neq 0 \qquad \text{And} \qquad \frac{dS}{dt} = 0, \qquad S \neq 0$$

With these formulations we can write the steady-state representation of rate equations (2.1) and (2.2).

$$\frac{\Gamma g_0(N_0 - N_T)S_0}{1+\varepsilon S_0} - \frac{S_0}{\tau_P} + \Gamma\beta\frac{N_0}{\tau_N} = 0$$

$$\frac{I_{DC}}{qV} - \frac{g_0(N_0 - N_T)S_0}{1+\varepsilon S_0} - \frac{N_0}{\tau_N} = 0$$

The steady state photon density from above, is given by

$$S_{DC} = S_0 = \frac{\Gamma\beta\dfrac{N_0}{\tau_N}}{\dfrac{1}{\tau_P} - \dfrac{\Gamma g_0(N_0 - N_T)}{1+\varepsilon S_0}}$$

If we consider the above threshold region of operation, the steady state carrier density is plugged to its threshold value and the stimulated emission is dominant in the cavity such that the below threshold spontaneous emission into the lasing mode is negligibly small. Thus, under these assumptions

$$\frac{S_0}{\tau_P} - \frac{\Gamma g_0(N_{TH} - N_T)S_0}{1+\varepsilon S_0} = 0$$

We neglect the gain compression term in the denominator, as its effect is very small

$$\Gamma g_0(N_{TH} - N_T) \approx \frac{1}{\tau_P} \tag{3.1}$$

This equation is consistent with our previous assumptions when describing the physical model of the semiconductor laser. Above threshold, the gain inside the cavity exactly equals the total cavity loss and is thus inversely related to the average photon lifetime, which defines the natural decay rate of the photons. Here, the use of a space-

independent model is justified as the implied assumption of equation (3.1) is in neglecting spatial dependence and assuming uniform field throughout the active region.

The DC component of the injected current can now be defined as the threshold current if we assume the photon density to be zero and plug this in to the carrier rate equation (2.2)

$$\frac{I_{TH}}{qV} \approx \frac{N_{TH}}{\tau_N} \tag{3.2}$$

Above threshold, the assumption of zero photon density is no longer applicable since the stimulated emission term is dominant and the photon density grows to its steady state value. The above-threshold steady state carrier rate equation (with $S \neq 0$), is given as

$$\frac{I}{qV} - \frac{g_0(N_0 - N_T)S}{1+\varepsilon S_0} - \frac{N_0}{\tau_N} = 0$$

$$\frac{I}{qV} - \frac{g_0(N_0 - N_T)S}{1+\varepsilon S_0} - \frac{I_{TH}}{qV} = 0 \qquad (\because \frac{N_{TH}}{\tau_N} = \frac{I_{TH}}{qV})$$

Making substitutions from equation (3.1) above

$$\frac{S_0}{\Gamma\tau_P} = \frac{I}{qV} - \frac{I_{TH}}{qV}$$

$$S_0 = \frac{\Gamma\tau_P}{qV}(I - I_{TH}) \tag{3.3}$$

Now, if we have defined the DC injection current as

$$I_{DC} = I_{TH} + I_B$$

$$\therefore S_0 = \frac{\Gamma \tau_P}{qV} I_B$$

Where 'I_B' is the above-threshold DC current component. This steady state relationship of the laser is represented by the *L-I* characteristic.

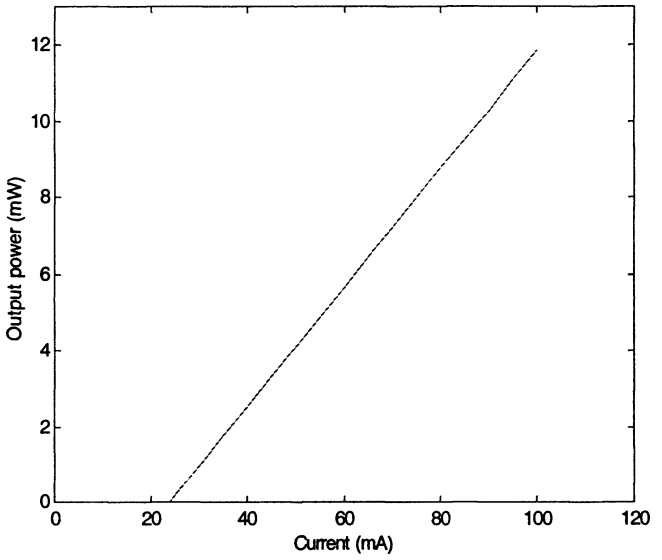

Fig.3.1 Typical steady-state L-I characteristic of a semiconductor laser

This is typical of most characteristics provided for commercially available devices. Note in particular the absence of any apparent photon density below the threshold point indicating absence of any spontaneous emission. However, in reality, a

very small level of light output is available below threshold, which is not represented by the *LI* characteristics.

3.2 Spontaneous emission and its effects on steady state characteristics

In any semiconductor laser, the threshold current I_{TH} is required to obtain the threshold carrier density, which is effectively clamped at this level for $I > I_{TH}$. Thus any injected electron in excess of the threshold current must contribute to the *stimulated emission* and the emitted power becomes proportional to $I - I_{TH}$. Below threshold, the laser emits spontaneous emission just like the usual LED. The total spontaneous emission power is given by [3].

$$P_{SP} = \eta_i \eta_R \frac{h\upsilon}{q} I$$

Where η_R is the radiative efficiency of the device. This is the power, which is available for all the laser modes below threshold. The below threshold region can be approximated by neglecting the stimulated emission term in photon rate equation above, and solving for S again under steady state condition, which gives:

$$S = \Gamma\beta \frac{N}{\tau_N} \tau_P$$

The output power through one laser facet is proportional to S and is given as [1]

$$P_0 = \frac{1}{2} v_G \alpha_M S h\upsilon V_P$$

Here $V_P = \frac{V}{\Gamma}$ and α_M is the mirror loss of the laser. On simplification, we obtain

$$P_{0(I<I_{TH})} = \eta_i \eta_R \left(\frac{\alpha_M}{\langle \alpha_i \rangle + \alpha_M} \right) \frac{h\upsilon}{2q} \beta I \tag{3.4}$$

α_i is the internal cavity loss.

$$\langle \alpha_i \rangle + \alpha_M = \Gamma g_{TH} = \frac{1}{v_G \tau_P}$$

Given that

$$\frac{1}{\tau_P} = \frac{1}{\tau_i} + \frac{1}{\tau_M}$$

The spontaneous emission has a low efficiency so that considerable optical power is emitted only after $I > I_{TH}$. Without the spontaneous emission, an absolutely abrupt transition at threshold would occur; however, due to the spontaneous emission term, one obtains an amplified spontaneous emission even below threshold, which depends on the amount of this emission in the lasing mode.

At threshold, the spontaneous emission clamps as the carrier density clamps since spontaneous emission rate (R_{SP}) depends upon N. Thus as current increases above threshold, the spontaneous emission noise remains constant at this value.

If we consider negligible feed back into the laser cavity then the feedback factor is unity and we can represent the output efficiency in terms of the cavity and mirror losses.

$$\eta_0 = \frac{\alpha_M}{\langle \alpha_i \rangle + \alpha_M}$$

Where η_0 is the output efficiency of the laser. The spontaneous output power is now given by

$$P_{0(I<I_{TH})} = \eta_i \eta_R \eta_0 \frac{h\upsilon}{2q} \beta I \qquad (3.5)$$

This also inherently explains the dependence of differential slope on the spontaneous emission factor. Higher the spontaneous emission captured by the lasing mode near threshold, less photons will be contributed towards stimulated emission (and in turn the output power) above threshold, thereby effectively decreasing the slope (remember, the internal efficiency for spontaneous emission is very small).

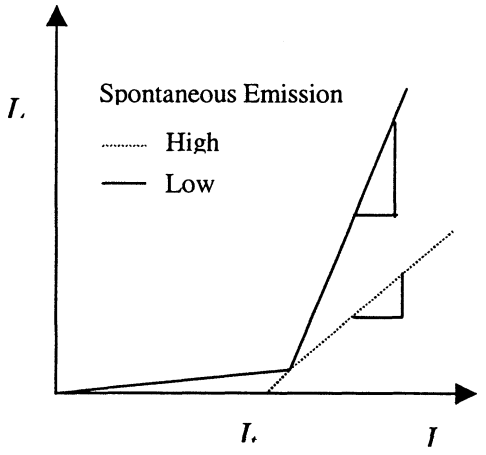

Fig.3.2 The effect of spontaneous emission on the differential quantum efficiency and in turn the slope

For DFB and DBR lasers, which by their very design are single mode lasers, this would be more apparent, since the mode suppression ratio (MSR) in these devices is much higher than their simple FP structure counterpart.

The ***L-I*** curve near threshold, which is approximated as a discontinuous change in the *L-I* slope, is more accurately a *'knee'* in the curve. This knee becomes softer for smaller devices (as indicated by the dashed curve in figure-3.2), due to the *higher* spontaneous emission rate in the lasing mode.

If non-radiative recombination is negligible, then as $\beta(N_{TH}) \rightarrow 1$, the threshold current reduces to zero. In such a "threshold-less" laser, *all* injected current is funneled into the lasing mode and we have maximum coupling of spontaneous emission into lasing (true for a LED). Thus the depth of the threshold of a laser governs the amount of spontaneously generated power that could couple into the lasing mode. For smaller devices where coupling is stronger, we have smaller values of threshold current together with a softer *'knee'* in the ***L-I*** characteristics.

3.3 A 'modified' rate equation model

We will now redefine the rate equations in such a way so as to reduce the total number of unknowns and will later show them to be self-consistently extractable from the steady state and small signal device measurements alone.

The two variables in the coupled rate equations are the carrier and photon densities and we can replace these variables with any other set of variables so that the transformation is valid as long as the process maintains the balance of terms in the original model. Through a proper combination of rate equation parameters, we develop a modified rate equation model in terms of lumped parameters, which constitute new but measurable combination of unknowns (Appendix-A).

$$\frac{dP}{dt} = \frac{\bar{a}(q(NV) - I_{TH}\tau_N)P + \frac{P}{\tau_P}}{(1 + \bar{a}\bar{b}\bar{c}\tau_P P_0)} - \frac{P}{\tau_P} + \beta(NV)\left(\frac{q}{\bar{c}\tau_P\tau_N}\right) \tag{3.6}$$

$$\frac{d}{dt}(NV) = \frac{I}{q} - \frac{\bar{a}\bar{c}\tau_P\left((NV) - \frac{I_{TH}\tau_N}{q}\right) + \frac{\bar{c}}{q}}{(1 + \bar{a}\bar{b}\bar{c}\tau_P P)}P - \frac{(NV)}{\tau_N} \tag{3.7}$$

$$\frac{d\phi}{dt} = \alpha\frac{1}{2}\bar{a}[q(NV) - I_{th}\tau_N] \tag{3.8}$$

Where

$$\bar{a} = \frac{\Gamma g_0}{qV} \quad ; \quad \bar{b} = \frac{\varepsilon}{g_0} \quad ; \quad \bar{c} = \frac{2q}{\eta_D h\upsilon}$$

The other three remaining unknowns are "τ_P", "τ_N"and "β". Thus we have reduced the total number of unknown parameters in the rate equation, from 9 to 6. We will now show that these parameters (or combination of parameters) are extractable from the steady state *L-I* characteristics and the small signal AM-response of the laser.

In formulating the modifications above we have invoked the assumption of uniform field distribution and in turn uniform carrier and photon density distribution across the active region of the laser. We also maintain that once threshold is achieved, the carrier density will remain clamped to its threshold value under steady state.

In the modified rate equations, it is important to note that the carrier density – volume product is shown in brackets, this is so because this product and not the carrier density alone, is used as a variable for solving the rate equations. Thus by combining the volume parameter with the carrier density, we, on one hand are able to eliminate this

parameter from the computation and on the other hand offer no significant modifications to the rate equation so as to affect the results.

3.4 Incorporating thermal effects

Temperature changes can be very detrimental to the operational stability of a laser. Rise in internal temperature may cause a drift in the operating wavelength and the *LI*-characteristics change. It is interesting to note the temperature dependent behavior of the steady state *LI*-curves for a typical laser model as shown in figure-3.3. When the device temperature increases, the ***L-I*** curve shifts outwards with an increase in threshold current. Both threshold current and internal efficiency are altered due to an increase in temperature, depending upon their respective characteristic temperatures.

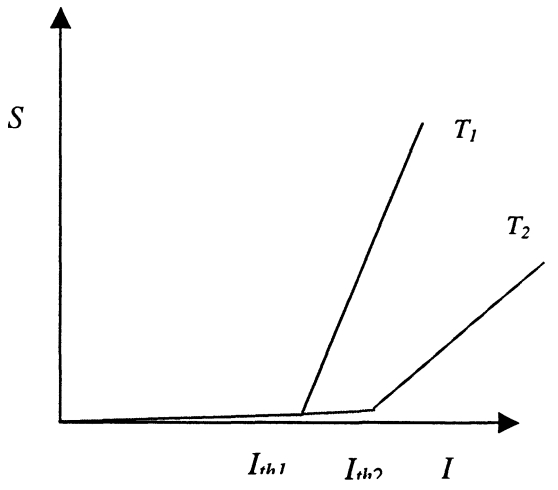

Fig.3.3 L-I curves as a function of temperature

There are no practical means to accurately measure the cavity temperature; only an estimate can be made based on the casing temperature. Typically, a cavity temperature will be 15-20% higher than the casing temperature. Available data that can be used to model thermal related behavior is thus from the steady-state behavior.

Thermal changes are very slow to set in as compared to the electronic transitions in the cavity. The thermal process time constant is in the range of a few hundred nanoseconds to several milliseconds [14], whereas the time constants of optical and carrier processes are in the order of nanoseconds. It is therefore difficult to incorporate the thermal effects directly into the time domain laser model, especially for the static state simulations. Thus, instead of incorporating thermal dynamics into our model we propose to predict behavior at any particular temperature assumed constant at that point in time and predicting behavior there of .

The strong thermal dependence can be attributed to many mechanisms. While auger recombination and optical losses can play a role in thermal behavior, the majority of affects during static or continuous wave operation are due to the temperature dependent laser gain and carrier leakage out of the active region.

Spatial hole burning due to carrier density changes, from temperature, can lead to further reduction of the injection efficiency. It is widely known that differential gain decreases with an increase in temperature and this dependence plays a dominant role in determining the thermal sensitivity of threshold current. The optical gain required to achieve lasing, has to compensate for the optical loss, which increases with increasing temperature, but to reach a higher gain, a higher carrier density is required. The carrier density dependence is introduced via the transparency carrier density using the same exponential function [12].

$$N_T(T) = N_{T0} \exp\left(\frac{\Delta T}{T_4}\right)$$

Where T_4 is the characteristic temperature.

All these interdependences are summarized through the bulk-cavity gain expression used in the standard rate-equations

$$G = \Gamma g_0 e^{-\frac{\Delta T}{T_1}} \left(N - N_T e^{\frac{\Delta T}{T_2}} \right)$$

The discussed mechanisms affect the static LI characteristics. The temperature related change observed in the steady state response indicate that the threshold current of the device increases (largely due to the auger affect), the external quantum efficiency decreases and the gain decreases at a higher rate, at higher output powers. We neglect auger recombination effects in determining the various parameters, which are computed from measurements taken at room temperature; hence, we also neglect the slight changes to such parameters as carrier and photon lifetimes, based on our assumption that information on gain, threshold current and external slope efficiency are sufficient to model steady state output characteristics due to temperature changes and that we can allow for reasonable margin of error in our estimated parameter values and still able to predict an accurate behavioral response.

By neglecting the effects of spatial hole burning, we can assume that the threshold current is simply a function of temperature. This empirical relation was first proposed by Panakov [13].

$$I_{TH(1)} = I_{TH(0)} e^{\left(\frac{\Delta T}{T_0}\right)} \tag{3.9}$$

We introduce this temperature dependence in the above-threshold steady state output power-injection current equation

$$P_0 = \eta_E \left(I - I_{TH(0)} e^{\left(\frac{\Delta T}{T_0}\right)} \right)$$

On comparison with our revised rate-equation model, we can observe that

$$\eta_E = \frac{1}{\bar{c}}$$

For the time being, we have ignored the thermal dependence of the external quantum efficiency. The change in this equation from the original relationship at room temperature is the decrease in out put power for the same level of injection current, implying an increase in leakage and cavity loss. If we thus, choose to decrease the injection current while maintaining the same threshold level then the effect should effectively be the same

$$P_0 = \eta_E e^{\left(\frac{\Delta T}{T_0}\right)} \left(I e^{-\left(\frac{\Delta T}{T_0}\right)} - I_{TH(0)} \right) \tag{3.10}$$

This implies that in order to maintain the same slope, the differential quantum efficiency need to be factored by the same multiplier as the threshold current.

P.Mena etal [5] has shown that by simply introducing the temperature related threshold offset current in the rate equation model we can predict the change in steady state response in VCSLs and the large signal dynamics due to a change in temperature without taking into account the thermal dependence of the differential quantum efficiency.

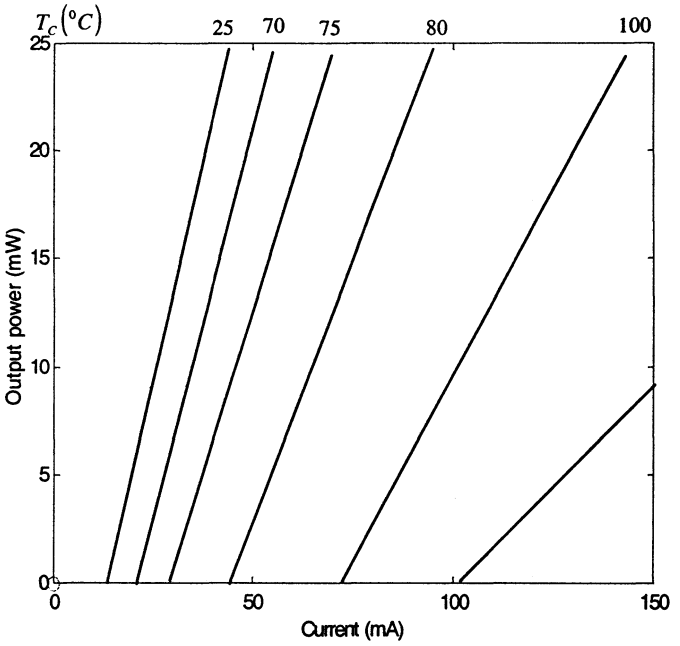

Fig.3.4 *Typical LI-curves for a 10-well, strained quantum well laser*

This may be true for the small VCSL cavity lengths but would not produce the same results with edge emitters as the external slope efficiency in edge emitting lasers exhibit a different thermal profile than that of threshold current. Thus the effect of slope changes in these devices cannot be ignored.

The gain changes due to temperature mainly determine the decrease in the external quantum efficiency and the increased compression at higher powers. It is observed from the LI-characteristics of many MQW and FP lasers that the thermally induced slope change occurs only at a particular casing temperature and not before. This behavior indicates the existence of a 'threshold' for the temperature dependent decrease

in the external slope efficiency of the laser. Figure-3.5 shows a typical example where the temperature threshold of the slope lies somewhere just below 70^0C.

Based on a similar approach as [5], we can predict the change in large signal behavior from temperature affects by using equation (3.10) but instead of a scalar thermal offset we introduce the exponential dependence of the threshold current to reduce the effective value of the injected current in the rate equation model. We do not ignore the temperature dependence of external slope efficiency as this information is built in our 'modified' model together with the threshold current, and can be used to predict the behavior of the steady-state *LI*-curves at higher temperatures.

Here, we propose that the thermal 'threshold' of the external slope can be predicted based on the characteristic temperature of the threshold current. As long as the temperature difference between room temperature and next higher temperature level is less than this characteristic temperature, the differential quantum efficiency of the laser will not have a thermal dependence, the external slope will effectively remain unchanged and equation (3.10) will be valid for all above threshold injection levels.

$$P_0 = \eta_E e^{\left(\frac{\Delta T}{T_0}\right)}\left(Ie^{-\left(\frac{\Delta T}{T_0}\right)} - I_{TH(0)} \right) \qquad \text{For} \qquad \Delta T < T_0$$

Or

$$\bar{c}\big|_{T_1} = \bar{c}e^{\left(-\frac{\Delta T}{T_0}\right)}$$

As described earlier, the same results are obtained in terms of output power if we introduce these changes in injection current and parameter $\bar{c}$, in the modified rate equation. But now, we also have the added advantage of predicting the device's large signal dynamic response to reflect the affects from temperature change.

$$\frac{dP}{dt}=\frac{\bar{a}\left(q(NV)-I_{TH}\tau_N\right)P+\dfrac{P}{\tau_P}}{\left(1+\bar{a}\bar{b}\bar{c}e^{\left(-\frac{\Delta T}{T_0}\right)}\tau_P P_0\right)}-\frac{P}{\tau_P}+\beta(NV)\left(\frac{q}{\bar{c}e^{\left(-\frac{\Delta T}{T_0}\right)}\tau_P\tau_N}\right)$$

$$\frac{d}{dt}(NV)=\frac{Ie^{\left(-\frac{\Delta T}{T_0}\right)}}{q}-\frac{\bar{a}\tau_P\left((NV)-\dfrac{I_{TH}\tau_N}{q}\right)+\dfrac{1}{q}}{\left(1+\bar{a}\bar{b}\bar{c}e^{\left(-\frac{\Delta T}{T_0}\right)}\tau_P P\right)}\bar{c}e^{\left(-\frac{\Delta T}{T_0}\right)}P-\frac{(NV)}{\tau_N}$$

When the temperature difference becomes equal to or exceeds the threshold current characteristic temperature, the external slope starts to decrease with increasing temperature and equation (3.10) is no longer valid. However, with a slight modification to the multiplying factor of parameter $\bar{c}$ in the rate equations, we can estimate the temperature dependent behaviors of the external quantum efficiency. The slope's thermal 'threshold' lies at the temperature where

$$\Delta T = T_0$$

$$\eta_E\big|_T = \eta_E e^{(1)}$$

Or $$\bar{c}\big|_T = 0.36\bar{c} \qquad \text{for all} \qquad \Delta T \geq T_0$$

Thus by using a constant factor based on the 'threshold' temperature, with parameter $\bar{c}$, we can estimate slope variations for all higher temperatures while maintaining the same thermal dependence of the injected current in the rate equations. The steady state changes due to temperature with the above modifications are given by

$$P_0 = 2.7182\eta_E\left(Ie^{-\left(\frac{\Delta T}{T_0}\right)}-I_{TH(0)}\right) \qquad \text{For} \qquad \Delta T \geq T_0$$

Whereas the large signal changes can be accounted for by bringing this dependence in the rate equations as before

$$\frac{dP}{dt} = \frac{\bar{a}(q(NV) - I_{TH}\tau_N)P + \frac{P}{\tau_P}}{(1 + 0.36\bar{c}\bar{a}\bar{b}\,\tau_P P_0)} - \frac{P}{\tau_P} + \beta(NV)\left(\frac{q}{0.36\bar{c}\,\tau_P\tau_N}\right)$$

$$\frac{d}{dt}(NV) = \frac{Ie^{\left(-\frac{\Delta T}{T_0}\right)}}{q} - \frac{\bar{a}\tau_P\left((NV) - \frac{I_{TH}\tau_N}{q}\right) + \frac{1}{q}}{(1 + 0.36\bar{c}\bar{a}\bar{b}\,\tau_P P)}0.36\bar{c}P - \frac{(NV)}{\tau_N}$$

We have presented a new method of introducing temperature related affects in the behavior of the laser from steady-state *LI*-curves at a minimum of two operating temperatures by using only the characteristic temperature of threshold current as the required parameter. The accuracy of estimate on this parameter is critical to the prediction of output at higher temperatures and if we continuously measure the external temperature, we can use this method to dynamically determine the output power even under CW operation.

In order to determine the wavelength chirp due to a change in temperature, the original phase rate equation is still a valid model, since the thermally induced increase (or decrease) in the carrier density is reflected in the variable *(NV)* in equation (3.8), which is reproduced here

$$\frac{d\phi}{dt} = \alpha\frac{1}{2}\bar{a}[q(NV) - I_{th}\tau_N]$$

We are able to account for all thermal effects within the linear region of operation above threshold, in the modified rate equations without introducing any complexity to the original model or imposing additional input data requirement.

3.4.1 Results from a commercial laser

We applied our thermal model to a Mitsubishi InGaAsP MQW-FP 1310nm laser (ML7xx8 series) where the steady state data at different temperatures was made available from the device data sheets. A set of parameters were arbitrarily selected to produce the desired output power, which are listed in table-3.1

Threshold current $I_{TH} = 5mA$

Characteristic temperature for threshold current $T_0 = 65^0 C$

Temperature 'threshold' for external slope $T_{TH} = 40^0 C$

Parameters	Unit	Value
τ_P	ps	2.0
τ_N	ns	0.1
$\overline{b}$	ps	8.5
$\overline{c}$	A/W	1.9
$\overline{a}$	GHz^2/mA	250
$\beta(1x10^{-4})$		0.44

Table-3.1

The characteristic temperature and the slope threshold temperature were based on data collected from the *LI*-curves only at two initial operating temperatures ($25^0 C$ and $50^0 C$) and the response at higher temperatures was then generated by the model.

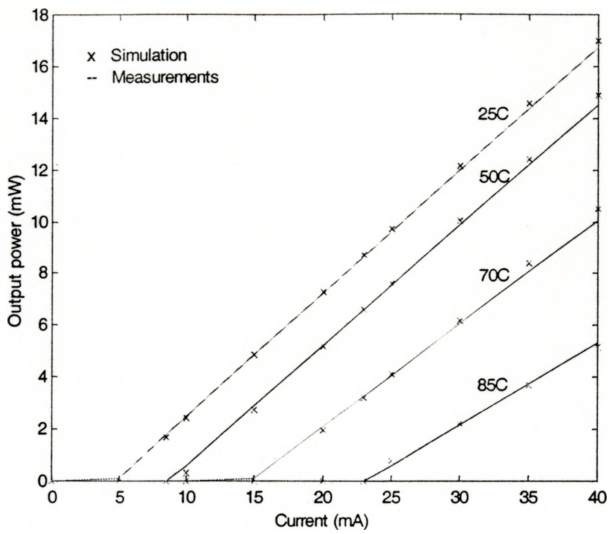

Fig. 3.5 A comparison of the output power estimated from the thermal model at different temperatures with actual device measured data

Note that for the measured temperatures, no change in slope was encountered but the model predicted the slope change at higher temperatures. The comparative results are shown in figure-3.5.

The large signal dynamics typically exhibit a reduced transient peak with increased damping and smaller resonance at higher temperatures. Simulations were carried out at $50^0 C$ and $70^0 C$ as shown in figure-3.6(a). A comparison with the results from a two-dimensional thermal model of a DFB-MQW laser, from a rigorous rate-equation modulation is shown in figure-3.6(b) and the dynamics are observed to be very much similar in both cases.

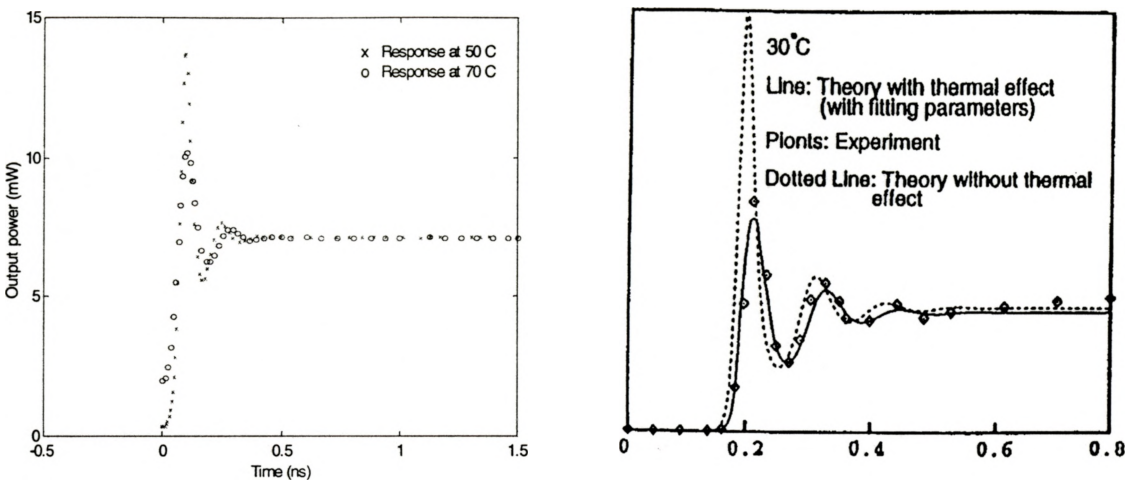

(a) (b)

Fig. 3.6 Similarity in large signal dynamics for single mode FP and DFB lasers (a) results from the Mitsubishi ML7xx8 series and (b) simulation of a MQW-DFB laser using a 2D standing wave model

In our analysis, we have ignored the affect of temperature on the modal parameters of the laser, as the steady state and large signal dynamics are directly modeled through the injection current and differential slope parameter. Thus, there is no apparent linkage of the introduced thermal affect to the small signal parameters, which are used to extract the intrinsic laser parameters in the first place and this implies that the affects are not depicted in the small signal response of the device.

Chapter-4

A Procedure For Extracting Rate Equation Parameters From Response Characteristics

4.1 Small signal analysis

Consider the application of an above threshold dc current I_0, superimposed with a small ac current I_1. Under steady state conditions the laser's carrier and photon density would respond similarly. Thus we can represent these in complex frequency domain notations

$$I = I_0 + I_1 \exp(j\omega t)$$

$$S = S_0 + S_1 \exp(j\omega t)$$

$$N = N_0 + N_1 \exp(j\omega t)$$

Making the assumption that:

1. Gain can be approximated as a straight line over the perturbation
2. The dc current is sufficiently far above threshold
3. Spontaneous emission is comparatively very small.

We analyze the rate equations by assuming that dynamic changes in the carrier and photon densities away from their steady state values are small. Taking the differential of both rate equations we can accommodate small signal responses of one variable in terms of a perturbation to another.

$$d\left[\frac{dS}{dt}\right] = d\left[\frac{\Gamma g_0 (N - N_T)S}{1+\varepsilon S}\right] - d\left[\frac{S}{\tau_P}\right] + d\left[\frac{\Gamma \beta N}{\tau_N}\right] \tag{4.1}$$

$$d\left[\frac{dN}{dt}\right] = d\left[\frac{I}{qV}\right] - d\left[\frac{g_0 (N - N_T)S}{1+\varepsilon S}\right] - d\left[\frac{N}{\tau_N}\right] \tag{4.2}$$

Solving for equation (4.1), we have

$$\frac{d}{dt}(dS) = \frac{(1+\varepsilon S_0)d[\Gamma g(N - N_T)S] - \Gamma g_0 (N_0 - N_T)S_0 d[1+\varepsilon S]}{(1+\varepsilon S_0)^2} - \frac{1}{\tau_P} dS + \frac{\Gamma \beta}{\tau_{\Delta N}} dN$$

Where the Carrier density, photon number and gain, outside the derivative are the steady state values and will be designated here as N_0, S_0 and g_0 respectively. $\tau_{\Delta N}$ is defined as the 'differential carrier lifetime' and has a carrier density dependence of the form

$$\frac{1}{\tau_{\Delta N}} \approx A + 2BN + 3CN^2$$

Where *'C'* is the auger recombination rate coefficient, *'B'* is the bimolecular recombination rate coefficient and *'A'* represents the non-radiative recombination coefficient. At normal (low) temperatures, the auger recombination is negligible and we recognize that for the best laser material the recombination at threshold is dominated by the spontaneous (bimolecular) recombination.

$$\frac{d}{dt}(dS)=\frac{(1+\varepsilon S_0)(\Gamma g_0(N_0-N_T)d[S]+S_0 d[\Gamma g(N-N_T)])-\Gamma g_0(N_0-N_T)\varepsilon S_0 dS}{(1+\varepsilon S_0)^2}$$

$$-\frac{1}{\tau_P}dS+\frac{\Gamma\beta}{\tau_{\Delta N}}dN$$

$$\frac{d}{dt}(dS)=\frac{(1+\varepsilon S_0-\varepsilon S_0)\Gamma g_0(N_0-N_T)dS+(1+\varepsilon S_0)\Gamma g_0 S_0 dN}{(1+\varepsilon S_0)^2}-\frac{1}{\tau_P}dS+\frac{\Gamma\beta}{\tau_{\Delta N}}dN$$

$$\frac{d}{dt}(dS)=\frac{\Gamma g_0(N_0-N_T)}{(1+\varepsilon S_0)^2}dS+\frac{\Gamma g_0 S_0}{(1+\varepsilon S_0)}dN-\frac{1}{\tau_P}dS+\frac{\Gamma\beta}{\tau_{\Delta N}}dN$$

Combining like terms on the RHS together, we have

$$\frac{d}{dt}(dS)=\left[\frac{\Gamma g_0(N_0-N_T)}{(1+\varepsilon S_0)^2}-\frac{1}{\tau_P}\right]dS+\left[\frac{\Gamma g_0 S_0}{(1+\varepsilon S_0)}+\frac{\Gamma\beta}{\tau_{\Delta N}}\right]dN \qquad (4.3)$$

Solving for equation (4.2) in a similar manner

$$\frac{d}{dt}(dN)=\left[\frac{1}{qV}\right]dI+\left[-\frac{g_0(N_0-N_T)}{(1+\varepsilon S_0)^2}\right]dS+\left[-\frac{g_0 S_0}{(1+\varepsilon S_0)}-\frac{1}{\tau_{\Delta N}}\right]dN \qquad (4.4)$$

Now, lets make the following associations

$$A\equiv\frac{\Gamma g_0(N_0-N_T)}{(1+\varepsilon S_0)^2}-\frac{1}{\tau_P}$$

$$B\equiv\frac{\Gamma g_0 S_0}{(1+\varepsilon S_0)}+\frac{\Gamma\beta}{\tau_{\Delta N}}$$

$$C \equiv -\frac{g_0(N_0 - N_T)}{(1+\varepsilon S_0)^2}$$

$$D \equiv -\frac{g_0 S_0}{(1+\varepsilon S_0)} - \frac{1}{\tau_{\Delta N}}$$

We can now write equations (4.3) and (4.4) in simple matrix notations

$$\frac{d}{dt}\begin{bmatrix} dS \\ dN \end{bmatrix} = \begin{bmatrix} A & B \\ C & D \end{bmatrix}\begin{bmatrix} dS \\ dN \end{bmatrix} + \frac{dI}{qV}\begin{bmatrix} 0 \\ 1 \end{bmatrix}$$

$$\frac{dI}{qV}\begin{bmatrix} 1 \\ 0 \end{bmatrix} = \begin{bmatrix} -A & -B \\ -C & -D \end{bmatrix}\begin{bmatrix} dS \\ dN \end{bmatrix} + \frac{d}{dt}\begin{bmatrix} dS \\ dN \end{bmatrix}$$

Based on our previous assumptions, we have solutions of the form

$$dS = S_1 \exp(j\omega t)$$

$$dN = N_1 \exp(j\omega t)$$

$$dI = I_1 \exp(j\omega t)$$

Setting $\frac{d}{dt} \rightarrow j\omega$ and rearranging

$$\frac{I_1}{qV}\begin{bmatrix} 1 \\ 0 \end{bmatrix} = \begin{bmatrix} -A + j\omega & -B \\ -C & -D + j\omega \end{bmatrix}\begin{bmatrix} S_1 \\ N_1 \end{bmatrix}$$

The determinant of the matrix is given by

$$\Delta \equiv \begin{vmatrix} -A + j\omega & -B \\ -C & -D + j\omega \end{vmatrix}$$

$$\Delta = AD - BC - (A + D)j\omega - \omega^2$$

We now use Crammer's rule to solve for the photon density.

$$S_1 = \frac{I_1}{qV}\frac{\begin{bmatrix} 1 & -B \\ 0 & -D + j\omega \end{bmatrix}}{\Delta}$$

$$S_1 = \frac{I_1}{qV}\frac{-D + j\omega}{\Delta}$$

If we describe the modulation response as a 2-parameter transfer function

$$H(\omega) = \frac{{\omega_0}^2}{\Delta} = \frac{{\omega_0}^2}{{\omega_0}^2 - \omega^2 + j\omega\gamma}$$

Then

$$S_1 = \frac{I_1}{qV}\frac{-D + j\omega}{{\omega_0}^2}H(\omega)$$

Where ${\omega_0}^2$ = Resonant frequency;

γ = Damping coefficient

Thus, by comparison we have

$${\omega_0}^2 = AD - BC$$

$${\omega_0}^2 = \left(\frac{\Gamma g_0(N_0 - N_T)}{(1 + \varepsilon S_0)^2} - \frac{1}{\tau_P}\right)\left(-\frac{g_0 S_0}{(1 + \varepsilon S_0)} - \frac{1}{\tau_{\Delta N}}\right) - \left(\frac{\Gamma g_0 S_0}{(1 + \varepsilon S_0)} + \frac{\Gamma\beta}{\tau_{\Delta N}}\right)\left(-\frac{g_0(N_0 - N_T)}{(1 + \varepsilon S_0)^2}\right)$$

$$\omega_0^2 = -\frac{\Gamma g_0^2 S_0 (N_0 - N_T)}{(1+\varepsilon S_0)^3} - \frac{\Gamma g_0 (N_0 - N_T)}{\tau_{\Delta N}(1+\varepsilon S_0)^2} + \frac{g_0 S_0}{\tau_P (1+\varepsilon S_0)} + \frac{1}{\tau_{\Delta N}\tau_P} + \frac{\Gamma g_0^2 S_0 (N_0 - N_T)}{(1+\varepsilon S_0)^3} + \frac{\Gamma \beta g_0 (N_0 - N_T)}{\tau_{\Delta N}(1+\varepsilon S_0)^2}$$

$$\omega_0^2 = \frac{g_0 S_0}{\tau_P (1+\varepsilon S_0)} - (1-\beta)\frac{\Gamma g_0 (N_0 - N_T)}{\tau_{\Delta N}(1+\varepsilon S_0)^2} + \frac{1}{\tau_{\Delta N}\tau_P} \tag{4.5}$$

$$\gamma = -A - D$$

$$\gamma = -\frac{\Gamma g_0 (N_0 - N_T)}{(1+\varepsilon S_0)^2} + \frac{1}{\tau_P} + \frac{g_0 S_0}{(1+\varepsilon S_0)} + \frac{1}{\tau_{\Delta N}} \tag{4.6}$$

4.2 Frequency response measurements and significance of measured parameters

In understanding the dynamic behavior of the laser, the variation in resonant frequency and damping factor provides useful insight into the intrinsic device parameters, which control the device behavior. These parameters can be easily obtained by fitting the small signal transfer function to the measured small signal response from a monochromator, given that the device operating frequency lies within the measurement range of the instrument. These experimental procedures and results are well documented [1],[2] and need not be detailed further. We will therefore restrict ourselves in the utilization of the extracted parameters of resonant frequency and damping coefficient, for computing (or estimating) the final rate equation parameters essential for large signal behavior modeling. The typical transfer function for the normalized small signal frequency response is shown in figure-4.1

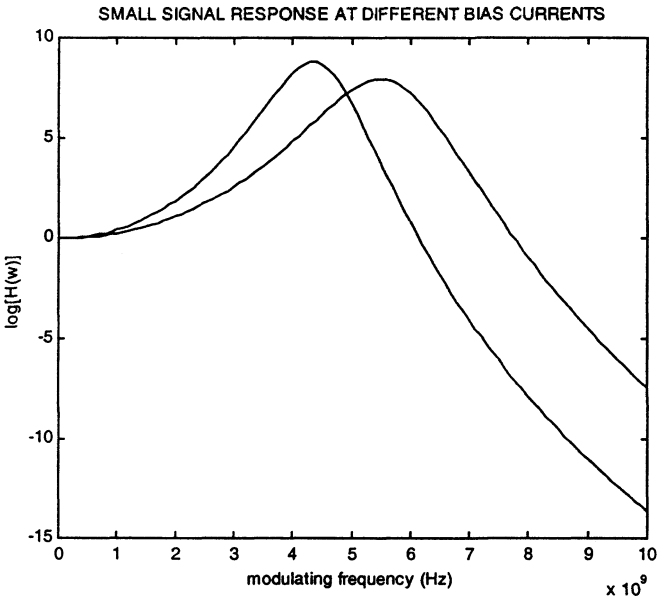

Fig.4.1 Variation in small signal response transfer function with changing bias current

With the increase in bias current, the response becomes more flat with the resonance frequency shifting forward. However, the resonant frequency is slightly higher than the peak response frequency and is described through the following relationship

$$\omega_p{}^2 = \omega_0{}^2 - 0.5\gamma^2$$

The resonance is damped at very low and high output powers. Beyond the strong resonance, the transfer characteristics degrade significantly. Thus effective modulation of the output power can only be achieved over a modulation bandwidth approximately $\approx \omega_0$. The modulation bandwidth of the laser can be steadily enhanced by increasing the output power, but is practically limited by:

a) Increased damping of the resonance at high powers

b) Thermal effects

c) High-power mirror facet damage

For a well-defined response curve at moderate bias levels, the peak frequency is quite well defined and from the transfer function relation of $H(\omega)$ and the above equation, the two variables can be easily extracted. There are several techniques, which could be used to measure frequency response accurately, each with its own associated problems. For standard laser diode chips, the device capacitance will dominate the frequency response at frequencies 10-20GHz needed to find the relevant laser parameters. The details of these measurement technique are beyond the scope of this report, however, we will describe a more recent 'Frequency Subtraction' method employed and its apparent advantages.

In frequency-subtraction method, the frequency response measurement just above threshold is subtracted from the frequency response measurement well above threshold. This eliminates all those measurement and device parameters, which do not vary with bias, leaving only the intrinsic response of the laser. Here it is assumed that the parasitic components of the laser are not power dependent. The subtracted response is given as:

$$\Delta H(\omega) = 10\log\left[\frac{{\omega_{01}}^2}{{\omega_{01}}^2 - \omega^2 + j\omega\gamma_1} x \frac{{\omega_{02}}^2 - \omega^2 + j\omega\gamma_2}{{\omega_{02}}^2}\right]$$

Where in this case we have four instead of two variables to fit the response curve. The typical subtracted frequency response is shown in figure-4.2 with the prominent maximum and minimum of the curve at the two ends of the measured frequency range.

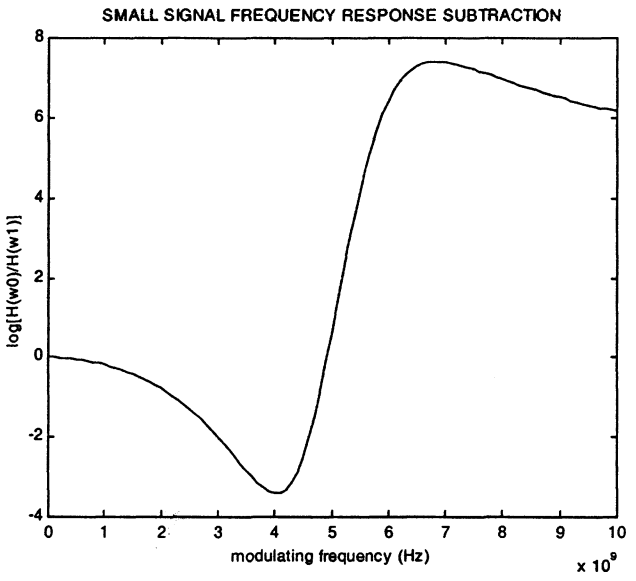

Fig.4.2 Typical Transfer function from frequency response subtraction at bias points close to threshold and well above threshold

Rewriting the double-pole modulation transfer function as the product of two single-pole transfer functions

$$H(\omega) = \frac{\omega_0^{\,2}}{\Delta} = \frac{\omega_0^{\,2}}{\omega_0^{\,2} - \omega^2 + j\omega\gamma} = \frac{\omega_0^{\,2}}{(j\omega + s_1)(j\omega + s_2)}$$

The roots of this function in the complex frequency plane are given by:

$$s_{1,2} = \frac{\gamma}{2} \pm j\omega_{osc}$$

Where

$$\omega_{osc}^2 = \omega_0^2 - 0.5\gamma^2$$

In some treatments, ω_0 is, by definition, set equal to ω_{OSC} and the damping factor is set equal to 0.5γ, to comply with the natural roots of the transfer function. The problem with making this equality is that the oscillation frequency (ω_{OSC}) becomes zero at high output powers. The standard definition (with ω_0) allows us to use the transfer function for small signal response at all powers (except for very small output powers). As for the damping factor, the alternate definition proves to be a better way to extract this parameter.

4.3 A Procedure For Parameter Extraction

In this section we will use the results previously derived from steady state and small signal analysis of the laser and systematically use these to predict reasonable estimates of the laser rate equation parameters for our modified model. The purpose here is not to find the 'exact' value of the parameters, but rather, to obtain values, which can accurately predict the behavior.

4.3.1 Differential quantum efficiency (η_D)

The differential quantum efficiency can be computed by solving the rate equations simultaneously at steady state using the following expression for photon density in terms of output power.

$$S(t) = \frac{2\Gamma\tau_P}{V\eta_D h\upsilon} P(t)$$

From equation (3.3)

$$S_0 = \frac{\Gamma\tau_P}{qV}(I - I_{TH})$$

Where we have assumed

$$1-\beta \approx 1$$

Making substitution for photon density

$$\frac{I}{qV} - \frac{2P}{V\eta_D h\upsilon} - \frac{I_{TH}}{qV} = 0$$

After some algebra, we get

$$\eta_D = \frac{2qP}{(h\upsilon)(I - I_{TH})} \tag{4.7}$$

The frequency term in the denominator can be approximated from the laser-operating wavelength, which is available with device data. All other terms are known from the characteristic *L-I* curve. It is evident from the above relation that the differential quantum efficiency defines the slope of the *L-I* curve at the point of measurement of output power. However, it has been observed that this slope may change for devices operating at too high injection levels or with high 'spatial hole burning' effects, as in the case of DFB or DBR lasers with $1/4\lambda$ phase shift in grating pitch. In such cases, this parameter will not be constant but vary with changing injection current and would have to be computed at every operating point.

4.3.2 Spontaneous emission coupling factor (β)

We have used β independently as a parameter as we will derive an expression for estimating its value directly from an analytical relationship of spontaneous emission at threshold. Spontaneous emission is of significance only below (and at) threshold levels of injection current. For commercial single mode lasers, this is reported negligible as indicated by their *L-I* characteristics. Here, however, *we assume that this spontaneous emission is not zero.*

For lasers operating below threshold, the output power close to threshold is the fraction of the total spontaneously generated power, since mode suppression ratio for single mode lasers is high and most of the photon resources will be employed by the lasing frequency having the lowest threshold gain requirement. Thus the total spontaneously emitted *'output'* power near threshold is in fact, the power that couples in to the mode of interest, or the lasing mode of the laser.

$$P_0(I < I_{TH}) = \beta P_{SP} \tag{4.8}$$

$$P_{SP} = \eta_i \eta_R (h\upsilon)\frac{I}{q} \qquad (I < I_{th})$$

By definition [3]

$$\beta \equiv \frac{R_{SP}'}{R_{SP}} = \frac{\Gamma v_g g n_{SP}}{\eta_i \eta_R \dfrac{I}{q}}$$

Where

$$R_{SP}' = \frac{\Gamma v_g g n_{SP}}{V} \qquad \text{and} \qquad R_{SP} = \eta_i \eta_R \frac{I}{qV}$$

In the above equation for spontaneous emission factor, n_{SP} is the 'population inversion factor'. Substituting for the spontaneous emission power, we obtain the relationship for the coupling factor.

$$\beta \equiv \frac{\Gamma v_g g n_{SP}(h\upsilon)}{P_{SP}}$$

Close to threshold

$$\Gamma v_g g_{th} \approx \frac{1}{\tau_P}$$

The spontaneous emission factor near threshold can be approximated by

$$\beta \equiv \frac{n_{SP}(h\upsilon)}{\tau_P P_{SP}}$$

Substituting this value in the equation (4.8) for output power below threshold, we have

$$P_0(I < I_{TH}) = \frac{n_{SP}(h\upsilon)}{\tau_P}$$

After comparing with equation (3.5), we get

$$\eta_i \eta_R \eta_0 \frac{h\upsilon}{2q} \beta I = \frac{n_{SP}(h\upsilon)}{\tau_P}$$

$$\beta = \frac{2qn_{SP}}{I_{TH}\tau_P \eta_i \eta_R \eta_0}$$

Near threshold, we have the following approximations

$\eta_R \approx 1$ [Since we assume at threshold $\frac{N_{TH}}{\tau_N} = \frac{I_{TH}}{qV}$, and]

$\eta_i \eta_0 = \eta_D$ [Where η_D is the differential quantum efficiency]

Thus

$$\beta = \frac{2qn_{SP}}{I_{TH}\tau_P \eta_D}$$

The population inversion factor n_{SP} ranges from 1-2, however for typical devices its value ranges between 1.5-2. For 1300nm InGaAsP lasers, the estimated value at room temperature is ~ 1.7. For all practical purposes, the value can be assumed to be the midpoint value; this would minimize the error of our estimation. Also, since the only other unknown parameter in the expression is the photon lifetime (τ_P), this value can be adjusted below 1.75 if the method used to calculate photon lifetime inherently underestimates it or, this value can be adjusted above 1.75 if the photon lifetime is known to be overestimated.

4.3.3 Lumped parameter of gain slope constant and cavity volume

The gain slope constant 'g_0', active region volume 'V' and the gain confinement factor 'Γ' are lumped together as a single unknown in the modified rate equation model. This lumped parameter can be directly obtained from the small signal resonant frequency 'ω_0' together with the steady-state *L-I* behavior at the given DC bias level. We know that the photon density is related to the output power from one facet of an AR coated device.

$$S(t) = \frac{2\Gamma\tau_P}{V\eta_D h\upsilon} P(t)$$

In equation (4.5) except for the first term on the RHS, all other terms collectively contribute only 2%-5% of the actual value of the function, assuming this contribution to be very small we can neglect these terms and approximate the function as

$$\omega_0^{\,2} = \frac{g_0 S_0}{\tau_P} \tag{4.9}$$

Where we have kept only the first term from the original expression, which is dominant in the linear region, using the approximation $1+\varepsilon S_0 \approx 1$. Substituting the value of S_0 above, we have

$$\omega_0{}^2 = \frac{g_0}{\tau_P} x \frac{2\Gamma \tau_P P_0}{V \eta_D h\upsilon}$$

$$\omega_0{}^2 = \frac{2\Gamma g_0 P_0}{V \eta_D h\upsilon} x \frac{q}{q}$$

$$\omega_0{}^2 = \frac{\Gamma g_0}{qV} x \frac{2P_0 q}{\eta_D h\upsilon} \tag{4.10}$$

From equation (4.7), we have

$$\frac{2P_0 q}{\eta_D h\upsilon} = I - I_{TH}$$

Substituting this expression in equation (4.10) gives us

$$\omega_0{}^2 = \frac{\Gamma g_0}{qV}(I - I_{TH})$$

$$\bar{a} = \frac{\Gamma g_0}{qV} \approx \frac{\omega_0{}^2}{I - I_{TH}} \tag{4.11}$$

The above equation indicates a linear relationship between above threshold injection current and the square of resonant frequency. However, close to threshold there is a non-linear variation in ω_0^2 and the parameter '$\bar{a}$' can achieve very high values. There is a very slight drift in the parameter value for injection levels sufficiently above threshold as the linear relationship of the above equation becomes valid, but nonetheless,

it remains uniform. For accuracy, the parameter '$\bar{a}$' need to be computed at every new bias, separately.

4.3.4 Spontaneous emission carrier lifetime (τ_N)

Rewriting equation (4.6) for the small signal damping coefficient

$$\gamma = -\frac{1}{\tau_P(1+\varepsilon S_0)} + \frac{1}{\tau_P} + \frac{g_0 S_0}{(1+\varepsilon S_0)} + \frac{1}{\tau_{\Delta N}}$$

Where, at steady state we have assumed $\frac{\Gamma g_0(N_0 - N_T)}{(1+\varepsilon S_0)} \approx \frac{1}{\tau_P}$

$$\gamma = \frac{\varepsilon S_0}{\tau_P(1+\varepsilon S_0)} + \frac{g_0 S_0}{(1+\varepsilon S_0)} + \frac{1}{\tau_{\Delta N}}$$

$$\gamma = \frac{\varepsilon S_0}{\tau_P} + g_0 S_0 + \frac{1}{\tau_{\Delta N}} \qquad (1+\varepsilon S_0 \approx 1) \qquad (4.12)$$

It was shown in chapter-3 that

$$\varepsilon S_0 = \tau_P \frac{\varepsilon}{g_0} x \frac{\Gamma g_0}{qV} x \frac{2P_0 q}{\eta_D h\upsilon} \qquad (4.13)$$

Solving with equation (4.10)

$$\varepsilon S_0 = \tau_P \frac{\varepsilon}{g_0} \omega_0^{\,2} \qquad (4.14)$$

Making substitutions from equations (4.9) and (4.14) in equation (4.12) above

$$\gamma = \frac{\varepsilon}{g_0}\omega_0^{\,2} + \tau_P\omega_0^{\,2} + \frac{1}{\tau_{\Delta N}}$$

$$\gamma = \left(\frac{\varepsilon}{g_0} + \tau_P\right)\omega_0^{\,2} + \frac{1}{\tau_{\Delta N}} \tag{4.15}$$

Similar to the standard equation of a line (considering linear functional relationship between the two small signal parameters) the expression is used to directly compute the differential carrier lifetime "$\tau_{\Delta N}$" from small signal IM frequency response measurements at a minimum of two bias points. The effective (differential) lifetime depends on the local slope of the spontaneous emission rate.

$$\tau_N \propto \frac{R}{N}; \qquad \tau_{N(eff)} \propto \frac{dR}{dN}$$

The dependence of total carrier lifetime, on carrier density has been expressed as

$$\frac{N}{\tau_N} = AN + BN^2 + CN^3 \tag{4.16}$$

From this relation we can directly compute the expression of differential lifetime, which appears, in our small signal analysis discussed earlier. Taking derivative of both sides of the equation

$$\left.\frac{1}{\tau_{\Delta N}}\right|_{TH} = A + 2BN_{TH} + 3CN_{TH}^2$$

The value for the total carrier lifetime can be evaluated at threshold as the carrier density is clamped to its threshold value. Therefore, dividing throughout by "N" in equation (3.16), we have the expression for total carrier lifetime (at threshold).

$$\left.\frac{1}{\tau_N}\right|_{TH} = A + BN_{TH} + CN_{TH}^2$$

Unless the laser is pumped too hard, the auger recombination is negligible since it is related to the temperature gradient of the cavity and for low injection levels, its affect is small enough to be neglected. If the non-radiative recombination in the cavity is minimal (which is true close to threshold), then the only other parameter of significance is the bi-molecular recombination, which also defines the spontaneous emission coupling in the lasing mode. This argument is especially valid for short wavelength lasers. With these underlining assumptions, the above equations are reduced to the forms

$$\left.\frac{1}{\tau_N}\right|_{TH} \approx BN_{TH} \qquad \text{And} \qquad \left.\frac{1}{\tau_{\Delta N}}\right|_{TH} \approx 2BN_{TH}$$

Thus the total carrier lifetime is approximately, *twice* that of the differential carrier lifetime.

4.3.5 Average photon lifetime and lumped gain compression parameter

From the previously derived equation (4.11), we know the following approximation

$$\omega_0^2 = \frac{\Gamma g_0}{qV}(I - I_{TH})$$

$$\omega_0^2 = \frac{\Gamma g_0 I_{TH}}{qV}\frac{(I - I_{TH})}{I_{TH}}$$

We add and subtract $\frac{1}{\tau_N \tau_P}$ from the RHS of the equation to yield

$$\omega_0^2 = \left(\frac{1 + \Gamma g_0 N_T \tau_P}{\tau_N \tau_P}\right)\frac{(I - I_{TH})}{I_{TH}} \qquad \left[\because \Gamma g_0 (N_{TH} - N_T) \approx \frac{1}{\tau_P}\right]$$

From this relation, we can compute the minimum value of photon lifetime, by setting the term $\Gamma g_0 N_T \tau_P$ equal to zero.

$$\omega_0^2 = \left(\frac{1}{\tau_N \tau_P}\right)\frac{(I - I_{TH})}{I_{TH}}$$

$$\tau_P\big|_{\min} = \frac{I - I_{TH}}{\omega_0^2 \tau_N I_{TH}}$$

$$\tau_P\big|_{\min} = \frac{1}{\bar{a}\,\tau_N I_{TH}}$$

The best possible value for photon lifetime can be based on the '*optimum design concept*' of the laser, assuming off course, that the laser is optimally designed for the application. Given the flexibility to adjust every cavity parameter, the optimization procedure would inevitably produce a design with unity mirror reflectivity and zero cavity length, since this design eliminates internal loss and creates the smallest possible mode volume. Practical designs however, are achieved when $L \to 0$ and $R \to 1$.

The knee of the gain curve (where *g/J* = *dg/dJ*) defines the optimum operating point for many design constraints and the threshold gain is placed closed to this point on

the curve (Appendix-B). The gain–carrier density relationship has been described either by an approximate linear function (which is used for most bulk lasers), or a more accurate logarithmic function. If we limit ourselves to positive gains ($g \geq 0$) only, this equation can be approximated as

$$g = g_0 \ln\left(\frac{N}{N_T}\right) \tag{4.17}$$

Where g_0 is the familiar differential gain coefficient. Assuming that the threshold lies at the knee of the gain curve as described above, then the threshold carrier density is given by

$$N_{TH} = eN_T$$

Bringing this dependence directly into our gain approximation used in the standard rate equation

$$g = g_0(N - N_T)$$

$$\Gamma g_0(N_{TH} - N_T) \approx \frac{1}{\tau_P}$$

Which is valid for all above threshold biases

$$\frac{1}{\tau_P} = \Gamma g_0\left(N_{TH} - \frac{N_{TH}}{e}\right)$$

$$\frac{1}{\tau_P} = \Gamma g_0 N_{TH}\left(\frac{e-1}{e}\right)$$

$$\frac{1}{\tau_P} = (0.632)\Gamma g_0 \frac{N_{TH}}{\tau_N}\tau_N$$

Using the assumption for threshold condition $\frac{N_0}{\tau_N} \approx \frac{I_{TH}}{qV}$

$$\frac{1}{\tau_P} = (0.632)\Gamma g_0 \frac{I_{TH}}{qV}\tau_N$$

$$\frac{1}{\tau_P} = (0.632)\bar{a} I_{TH}\tau_N \qquad \text{[Where } \bar{a} = \frac{\Gamma g_0}{qV}\text{]}$$

$$\tau_P = \frac{1.582}{\bar{a} I_{TH}\tau_N} \tag{4.18}$$

Including the constraint of maximum differential gain for high-speed lasers, as described in Appendix-B, we move down the curve towards transparency, to obtain the maximum estimated photon lifetime corresponding to the maximum (optimum) cavity length.

$$\tau_P\big|_{opt} = \frac{1.8984}{\bar{a} I_{TH}\tau_N} \tag{4.19}$$

Either equation (4.18) or (4.19) can be used to estimate this parameter without causing any significant change in behavior. However, assuming that the laser is designed for high-speed data applications, the latter gives a better estimate for the model. Equation (4.14) implies a straight line relationship between the small signal parameters "γ" and "$\omega_0^{\,2}$"and the slope of this line gives us the sum of the two required parameters.

$$K = 4\pi^2\left(\frac{\varepsilon}{g_0} + \tau_P\right)$$

This slope would effectively give us the range within which the average photon lifetime above threshold would exist for any particular laser. After substituting this value of τ_P in the *'K-factor'*, we can directly compute the remaining parameter '$\bar{b}$'.

4.4 Large signal analysis

To determine the dynamic response of the laser for large-signal inputs we need to solve the rate equations iteratively using a numerical solver with a small increment of time Δt in place of dt. We use a regulation step input current pulse for the simulation, mainly for two reasons. First, it is easier to implement in to the program's sub-routine, secondly, since we are not making comparison with any measured signal, we are avoiding all the noise sources extraneous to the laser (e.g. due to the mounting fixture etc.), which might interfere with the response. Also, an instantaneous transition of current pulse will include all the frequency harmonics and the prominent 'ringing' affect at the output can be easily related to the small signal parameters of resonant frequency and damping coefficient. A variable 2nd order and 3rd order Runge-Kutta method is employed to solve these equations. We carry out the analysis for the following two bias conditions.

a. Lasers pre-biased above threshold.
b. Lasers pre-biased below threshold.

The reason for this differentiation is based on the fact that below threshold information for the laser is not built into our rate equation model and the dynamics are vastly different under the two bias conditions, for different laser types. Firstly, turn-on delays are avoided once the laser is subjected to an above threshold initial bias before the

application of input (signal), secondly, all the modal parameters are relatively fixed once threshold is achieved, below threshold, the governing relationships for the parameters are no longer valid and there is no means to model the unique below-threshold dynamics on a case-to-case basis. For example, the rate equation model does not explain the observed difference in peak amplitudes of the response [2] when the laser is 'cold' started with zero (or less than threshold) initial bias. Here, we attempt to account for these behavior by modifying the related modal parameter in our model under the two cases.

4.4.1 Case (a) - Above threshold bias condition

It can be shown that for lasers biased above threshold, the turn on delay is negligible. Considerable optical power is emitted only after $I > I_{TH}$. Beyond threshold the stimulated emission accounts for the nearly uniform transition without delay.

If the laser is always kept above threshold, the carrier density does not change by a large amount due to carrier clamping, even during large transients. Thus, the assumptions made under small signal analysis remain valid under the large signal regime.

With a greater-than-threshold initial bias, the carrier density is already clamped at its final (average) value and any additional current from the input simply tends to oscillate the carrier profile about this mean. The phenomenon as shown in figure-4.3 is for a DFB laser for bias currents of 30mA to 50mA with a (above-threshold) pre-bias level of 20mA before applying the input. The initial rate of change defines the carrier lifetime inside the cavity.

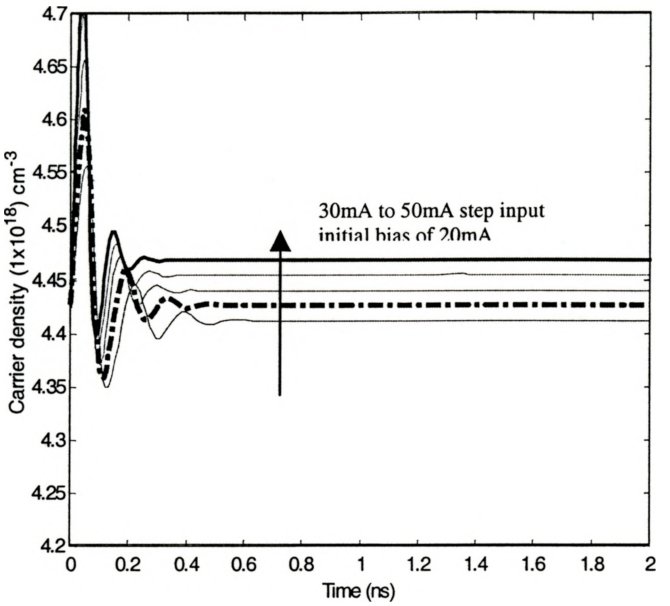

Fig.4.3 Variation of the carrier density in response to a range of step input signals for a laser biased around 20mA ($I_{threshold}$=18mA)

We can approximate the net change in carrier density to be negligible (since this variation is vary small compared to the absolute value). For lasers with operating point above threshold, the large signal variations in the excess carrier density would always start from the same initially clamped threshold value, whose absolute value would be much higher than the changes in the density profile itself. Thus, the choice of carrier lifetime (differential or total) in the model would have little or no affect on the output.

4.4.2 Case (b) - Below threshold bias condition

Turn-on delay of the laser depends on the absolute change in the carrier density inside the cavity, which in turn relates to the decay rate of the carrier (to produce

photons) defined by their lifetime, thus, smaller the lifetime, smaller would be the total carrier build up.

This difference in carrier density would however, not affect the steady state photon density value, as $\frac{N}{\tau_N}$ or $\frac{N}{\tau_{\Delta N}}$ terms in the rate equation would be the same since the difference in life time values would be compensated by the proportionate difference in the carrier density values.

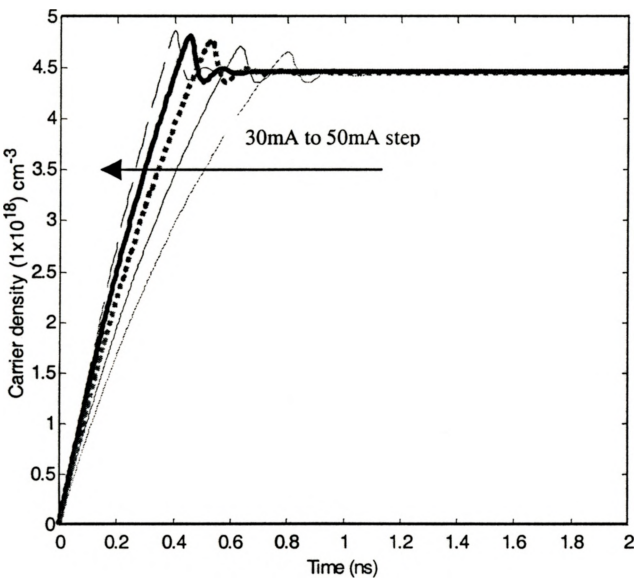

Fig.4.4 Variation of the carrier density in response to a range of step input signals for a laser with zero initial injection current

When the laser is at zero injection level prior to the application of the input, the *addition* to the carrier density in conduction band is supposedly zero (off course there are small changes in the carrier population always taking place, not attributed to the injected

current and not accounted for). If a step input is applied to the laser the 'additional' carrier density due to this input, starts to build up almost linearly until it is clamped when the laser reaches threshold.

Figure-4.4 shows the comparison between the carrier density profiles for each level of injection current for the same DFB laser, the average density in the cavity is around $4.43x10^{18}$ carriers per unit volume, at nearly all bias levels and there is not much difference between the initial slopes of the curves except for the bias level close to threshold.

Most device operating points are kept well above threshold to avoid noise interference due to mounting fixture capacitances and other non-linearities near threshold. Thus, we can assume an average value of the initial rate of change in carrier density based on the final (average) value of the carrier density, which is the 'clamped' steady state value.

As a first approximation to estimate the turn-on delay, we can calculate the initial slope of the carrier density and draw a straight line up to the threshold value N_{TH}. Using the carrier rate equation and assuming no significant photon build-up

$$\frac{dN}{dt} = \frac{I}{qV} - \frac{N}{\tau_N}\bigg|_{Spont}$$

If there is some initial current (say I_i), then the spontaneous emission term under steady state can be set equal to

$$\frac{N}{\tau_N}\bigg|_{Spont} = \frac{I_i}{qV}$$

Thus the initial slope is

$$\left.\frac{\Delta N}{\Delta t}\right|_{t=0} = \frac{I - I_i}{qV} = \frac{N_{TH} - N_i}{t_d}$$

$$t_d = \frac{qV(N_{TH} - N_i)}{I - I_i}$$

$$t_d = \frac{qV(N_{TH} - N_i)}{I - I_i} x \frac{\tau_N}{\tau_N}$$

Now, we know that around threshold $\frac{N_{TH}}{\tau_N} \approx \frac{I_{TH}}{qV}$

Thus, using the same dependence for any intermediate carrier density level (assuming that the non-radiative recombination is minimal)

$$\frac{N_i}{\tau_N} \approx \frac{I_i}{qV}$$

Hence, by substitution

$$t_d = \tau_N \frac{(I_{TH} - I_i)}{(I - I_i)}$$

If the initial injection current and carrier density are both assumed zero, then

$$t_d = \frac{qV(N_{TH})}{I}$$

$$t_d = \tau_N \frac{I_{TH}}{I} \qquad \left(\frac{I_{TH}}{qV} = \frac{N_{TH}}{\tau_N}\right)$$

Note that the turn-on delay, for both cases, is dependent on the total carrier lifetime and not the differential lifetime of the laser. Thus, if the laser starts from a below threshold bias, the absolute change in carrier density is quite significant and the spontaneous emission (total) carrier lifetime would be required to predict turn-on delay.

Below threshold, spontaneous emission contribution is the only source of photon build-up inside the cavity and the above threshold transients are directly linked to the amount of photons made available from spontaneous emission, before the laser starts lasing.

We already have estimation for carrier lifetime. Without altering other parameters (whose change in values have little or no affect on the response), intuitively, if we are able to account for the below threshold contribution from lasing mode spontaneous emission alone, we should be able to predict the response. However, there is no way of knowing the exact profile of these contributions. Since all below-threshold contributions add on to the cumulative photon build-up to threshold, we can assume a constant amount of photon emission, which is an average value of the total contribution. This approximation can be made by empirically introducing a multiplier in the rate equation, such that

$$\beta\big|_{I<I_{TH}} \approx m\beta\big|_{I\geq I_{TH}}$$

$$\beta\big|_{I\geq I_{TH}} \approx \sum_{t_0}^{t_{TH}} \beta_{av}$$

Where "m" is generally of the order of 10^{-5} and β_{av} is based on the solver time steps and the estimated value of β at threshold. The validity of this method is tested on the ALDH model and shows very good results with a quarter-wave shifted DFB laser (chapter-5).

Chapter 5

Model Testing and Verification

5.1 Measurements

To validate the parameter extraction procedure, we have utilized data from two different sources. To avoid experimental errors and to provide common grounds for comparison of results we have used data that has already been validated by other models or methods. In the first case, we used fitted values of resonant frequency and damping coefficient obtained from measured small signal response of a MQW-DFB chip-on-carrier laser mounted in a butterfly package and having a threshold current of 18mA. The configuration had a mount-limited bandwidth of 2.5Gbps and an operating wavelength of 1550nm as reported in [1].

This laser is designated here as 'laser-A'. It is shown to provide excellent results from simulations using the numerical optimization routine by J.Cartledge etal. and is claimed to produce a sum of squared errors of 10^{-12}, which is quite accurate. The same data has been used to compute parameters as described above. Here, we will compare the results from the two methods. We also compare the computed parameters from the two methods to show the relative margin of difference and the similarity at different bias points. Laser-A thus provides us with a testing platform to compare the parameter

extraction method with another documented method and at the same time evaluate response results from two essentially similar models.

In the second case we employ a more rigorous verification method. Here we will use the Advanced Laser Diode Simulator (ALDS) (courtesy Apollo Photonics Inc.). This simulator is based on a physics-based quasi-3D model which is fundamentally different from the 0D behavioral models used for the parameter extraction, yet it generates the steady state and small signal data similar to the commonly measured data available from most vendors and also carry out large signal simulations based on pre-defined structural parameters that are fed into the model. This type of simulation is a very useful alternate to actual measurements from real devices, as the results are free from extraneous noise interferences and produces a behavioral response that can be traced back to the device's physical characteristics such as cavity length, volume, thickness etc., which are treated as fixed input constants instead of unknowns. Furthermore, the results will demonstrate shortcomings of a simple 0D model in comparison with a much more complex 3D model

For the purpose of verification, we have used an AR-coated index-coupled quarter-wave shifted InGaAsP/InP DFB laser, having an active cavity length of 300 μm, a threshold current of 23.8mA and an operating wavelength of 1658.3nm. The model laser is designated as 'laser-B'. Some problem is encountered with spatial hole burning effects, which become prominent for bias currents well above threshold and tend to increase the slope of the *LI*-curve within the linear operating region.

5.2 Procedure for comparison and verification

Our method of parameter extraction derives directly from the small signal and steady-state parameters; therefore the model would invariably give accurate reproduction

of these two characteristic behaviors. The main test of the method lies in predicting response to large signal inputs.

From the measured values of injected current and output power, we directly determine the threshold current and parameter '$\bar{c}$' using 2-parameter curve fitting through implementing the **polyfit** function in Matlab. Alternately, we can also compute the two unknowns from the 2-point form equation of a straight line. Using the same straight-line approximation on the square of resonant frequency and damping coefficient, we obtain the differential carrier lifetime and the '*K-factor*' slope, which gives us the sum of the average photon lifetime and parameter '$\bar{b}$'.

The total spontaneous emission carrier lifetime is simply twice the differential lifetime. From the optimum design constraint for high-speed lasers, we predict the optimum probable value for the photon lifetime (and in turn the cavity length) at different bias currents and using the computed value of the *K-factor*, determine the parameter '$\bar{b}$'.

Parameter '$\bar{a}$' is obtained from the resonant frequency and the injected current above threshold as per equation (4.11), while the spontaneous emission coupling factor is computed directly from the values of photon lifetime, threshold current and differential slope efficiency with an estimated population inversion factor of 1.75.

5.3 Comparisons in 'Laser-A'

A set of measurements at different bias conditions has been provided in [1], which here are assumed accurate for the sake of comparison. A frequency response subtraction process, (as discussed in chapter-4) has been used to extract the small signal response parameters at any particular input bias point.

The small signal transfer function used here for the curve fit is

$$H(\omega) = \frac{Z}{Z - \omega^2 + j\omega Y}$$

Where 'Z' and 'Y' are the functions of the device resonant frequency and damping factor, given by

Damping factor $\Gamma = Y$

Square of resonant frequency $\omega_0^2 = Z - \frac{1}{2}Y^2$

The frequency responses for different bias currents were measured using light wave component analyzer (HP8703A). An intensity modulation response, at bias currents of 23mA was subtracted from an IM response at 35mA bias current and another at 45mA bias current. Sum-of-squared-errors criterion was used to fit the curves so obtained, to the transfer function given above, minimized over the four variables (from the two subtracted responses) using a quasi-Newton method and a finite difference gradient. The results of this minimization were not found to be sensitive to initial estimates.

Parameters	**Bias current (mA)**					
	25	**30**	**35**	**40**	**45**	**50**
$P_1(mW)$	0.56	0.97	1.36	1.73	2.16	2.55
$Y_1(x10^9\ \mathrm{sec}^{-1})$	12.16	16.96	21.87	25.91	30.35	35.12
$Z_1(x10^{20}\ Hz^2)$	8.96	14.79	20.52	26.03	31.00	35.71
$\omega_0^2(x10^{20}\ Hz^2)$	8.22	13.35	18.12	22.67	26.4	29.54

Table-5.1

Table.5.1 lists the values of measured small signal response parameters at different bias currents, the exact value for the square of resonance frequency as per the given relation is also computed and shows an increasing departure from the approximate value with increasing bias levels.

5.3.1 Discussion on extracted parameters in [1]

The minimization for the numerical optimization method of [1], is reportedly over the original nine rate equation parameters to simultaneously yield the measured values above. The values of the parameters so obtained show a weak dependence on the bias current which has been attributed to experimental uncertainty. The minimization routine finds a local minimum with a sum of squared errors of around 10^{-12}, which is considered quite accurate.

However, the minimization over all the nine parameters was found to be very difficult and the results indicated that a single set of rate equation parameters does not simultaneously satisfy the given constraints with sum of squared errors as high as 10^{-2}. This implied that the initial estimates had to be chosen very carefully in order the minimization to converge.

The parameters, 'ε' (gain compression factor), 'V' (active cavity volume), and 'g_0' (gain slope constant) had shown the most variation during the 25mA to 50mA transition of the input bias. All other parameters exhibited only a slight adjustment. Also, the initial estimates are very close to the minimized values of the parameters indicating the sensitivity of the process. For the purpose of comparison table-5.2 lists the parameters for our modified model from the originally computed parameters in [1].

Parameters	Initial Estimates	Bias Current (mA)					
		25	30	35	40	45	50
$\bar{a}(GHz^2/mA)$	-	128	125	120	122	116	115
$\bar{b}(x10^{-12}s)$	-	11.10	9.81	9.31	8.71	8.64	8.76
$\bar{c}(A/W)$	-	12.49	12.49	12.49	12.49	12.49	12.49
$\tau_P(x10^{-12}s)$	1.0	0.78	0.79	0.79	0.8	0.8	0.81
$\tau_N(x10^{-9}s)$	1.0	0.74	0.75	0.76	0.77	0.78	0.79
$\beta(x10^{-4})$	1.0	1.01	1.00	1.00	1.00	1.00	1.00
$N(x10^{18}cm^{-3})$	4.4	4.44	4.35	4.36	4.39	4.43	4.49
$S(x10^{14}cm^{-3})$	10.0	4.5	7.44	10.27	12.82	15.52	18.24
$I_{TH}(x10^{-3}A)$		18.0	18.0	18.0	18.0	18.0	18.0
$P_1(x10^{-3}W)$		0.56	0.97	1.36	1.73	2.16	2.55

Table-5.2

Parameter '$\bar{b}$' as obtained from the numerical optimization, show a steep decline from its initial value to the final value at 50mA with a variation of nearly 20% to the base value at 25mA bias current. Parameter '$\bar{a}$' on the other hand varies a bit erratically over the bias range, these variations may be attributed to the adjustment mechanism of the minimization subroutine to find a local minimum on or around the initial estimate.

The large signal response simulations using the parameters at 35mA and 50mA have shown quite identical results as reported in [1]. The sufficiently large difference in values of the parameters over the entire range of injection current shows that we have a reasonably good margin of error in estimating parameters '$\bar{a}$' and '$\bar{b}$' as compared to determining uniquely optimized solutions to the nine parameters of the original rate equations, as is the case in [1].

5.3.2 Estimation of parameters using the proposed method

From the measured values of injected current and output power we directly determine the threshold current and parameter '$\bar{c}$' using 2-parameter curve fitting. The fitted value of threshold current stands at 17.9mA and the output slope efficiency at 0.198. Both these values are very close to the reported values.

Arbitrarily selecting a range of measurement within the linear operating region above threshold, we use the same straight-line approximation on the square of resonant frequency and damping coefficient to obtain the differential carrier lifetime and the '*K-factor* 'slope, which gives us the sum of the average photon lifetime and parameter '$\bar{b}$'. The total spontaneous emission carrier lifetime is set as approximately twice the differential lifetime. Under the optimum design constraint (Appendix-B), we predict the optimum probable value for the photon lifetime (and in turn the cavity length) at different bias currents and using the computed value of the *K-factor*, determine the parameter '$\bar{b}$'.

Parameter '$\bar{a}$' is obtained from within the selected range of resonance frequency and the injected current above threshold from approximated solution of equation (4.9), while the spontaneous emission coupling factor is computed directly from the computed parameters with an estimated population inversion factor of 1.75. The parameters so obtained are listed in table.5.3.

The relationship between the resonance frequency and above threshold injection current is sub-linear. However, the relationship between the square of resonance frequency and current is very much linear as shown in figure-5.1, and this forms our basis for estimation of parameter '$\bar{a}$' over a range of measured values at different injection levels.

Parameters	Initial Estimates	Bias Current (mA)					
		25	30	35	40	45	50
$\bar{a}\left(GHz^2/mA\right)$	-	117	111	107	103	98	92
$\bar{b}\left(x10^{-12}s\right)$	-	9.15	9.07	9.01	8.96	8.88	8.78
$\bar{c}\left(A/W\right)$	-	12.59	12.59	12.59	12.59	12.59	12.59
$\tau_P\left(x10^{-12}s\right)$	-	1.36	1.43	1.49	1.55	1.63	1.73
$\tau_N\left(x10^{-9}s\right)$	-	0.66	0.66	0.66	0.66	0.66	0.66
$\beta\left(x10^{-4}\right)$	-	1.16	1.1	1.06	1.02	0.97	0.91
$I_{TH}\left(x10^{-3}A\right)$		17.9	17.9	17.9	17.9	17.9	17.9
$P_1\left(x10^{-3}W\right)$		0.56	0.97	1.36	1.73	2.16	2.55

Table-5.3

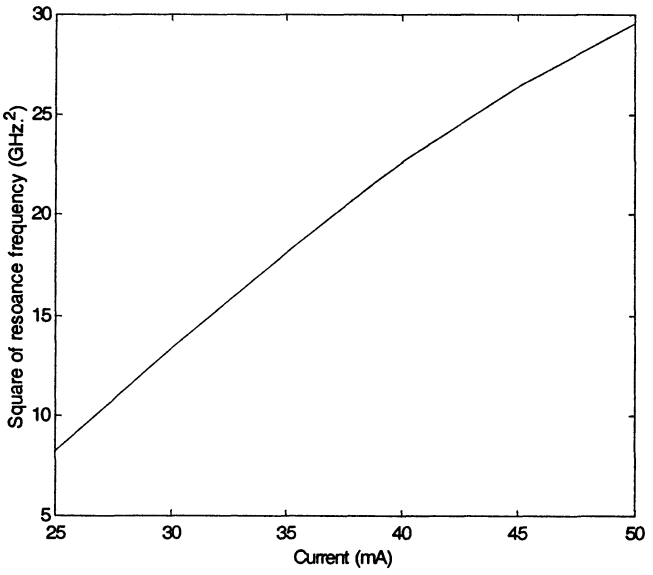

Fig.5.1 Plot showing the near linear relationship between the square of resonance frequency and injection current

The measured and calculated values of the damping coefficient are shown in figure-5.2. to verify the self-consistency of the method. Except for very small discrepancies at 40mA and 50mA bias currents, the computed data compares well with the measured small signal parameters. The procedure involves solving equation (4.5) and equation (4.6) from the estimated parameter values and comparing the results with the measured small signal parameters.

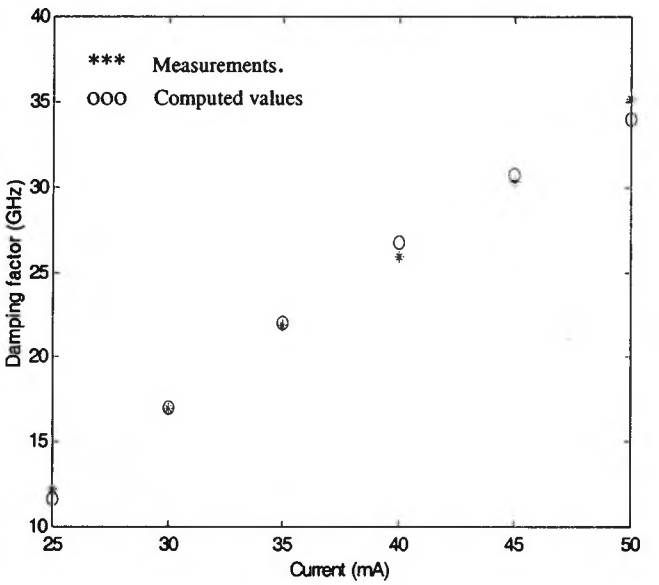

Fig.5.2 Comparison of measured and calculated values of the damping factor (small signal parameter) at different bias currents.

Resonance frequency as a function of the damping coefficient gives us a *K-factor* of approximately 0.415ns and the measured value is 0.4ns, whereas the value computed through the numerical approximation method of [1] is reported at 0.49ns. Figure-5.3 shows this comparison at different bias levels. The slope of the line joining the data points gives us the *K-factor*. The same procedure is adopted here as described earlier.

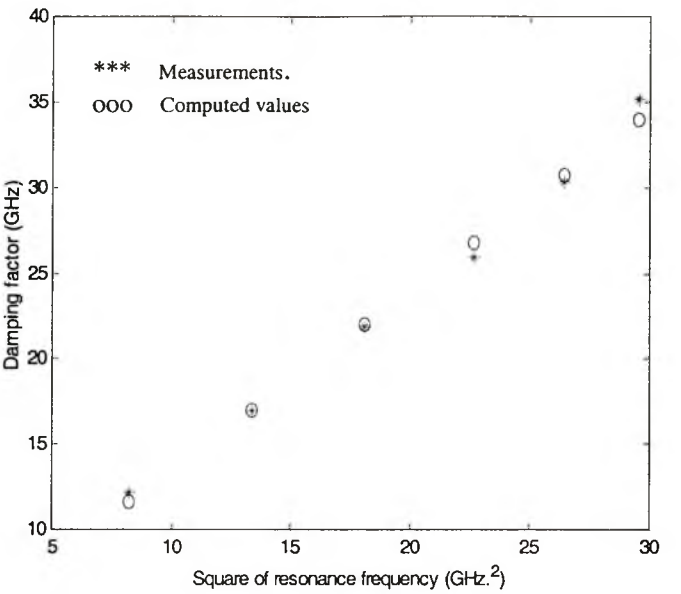

Fig.5.3 Measured and computed values of the K-factor

5.3.2 Comparison of results from the two methods

The computed parameter '$\overline{a}$' is lower than that estimated in [1], but since the absolute value of this parameter is the maximum of the lot (of the order of $1x10^{23}$), the difference is not found to be significant for the purpose of characterizing behavior.

Since we have used a linear relationship to compute this parameter, we can therefore predict (and observe) a near uniform drift with increasing injection current, on the other hand the values computed from the numerical optimization have a non-uniform drift with obvious kink at 40mA. The important similarity to note is that in both cases the value decreases with increasing injection levels.

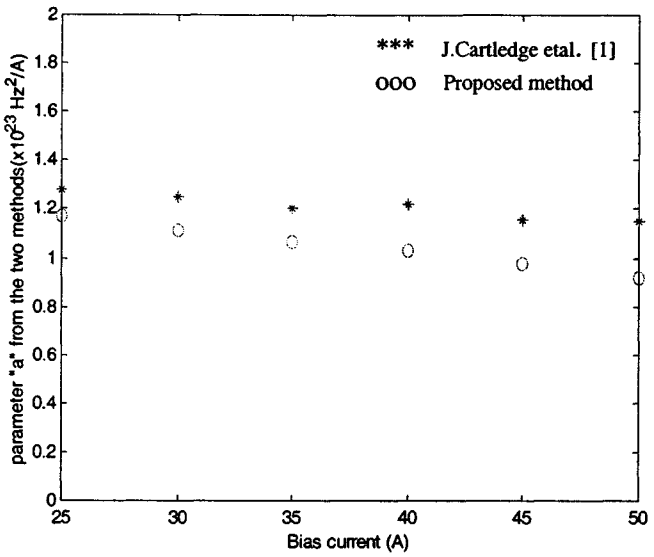

Fig.5.4 A comparison between computed values of '$\bar{a}$' from the two methods, the values are decreasing with increasing bias in both cases.

Figure-5.5 shows the total carrier lifetime, which is twice the differential lifetime, computed from the small signal response, and based on the assumption that there is no auger recombination present. The values so obtained are slightly lower than those reported in [1]. This difference affects the turn-on delay in both cases when we go on to compare large signal response for the laser with zero bias or when biased below threshold before the application of the signal. A very slight drift in this parameter values from [1] indicates a near uniform carrier lifetime at all injection levels.

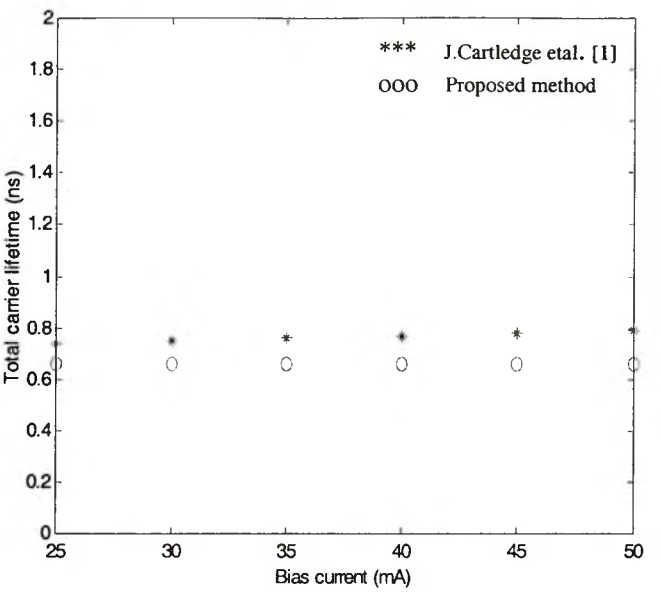

Fig.5.5 The absolute difference between the computed values of carrier lifetimes may be small but it affects the turn-on delay of the laser, when it is pre-biased below threshold

Figure-5.6 shows the differential slope efficiencies from the two methods. As indicated earlier, the two values are very close to each other and this may not be of concern at bias points close to threshold (above threshold) but if the large signal input, especially, a step input forces the bias well above threshold or if the operating point of the laser lies sufficiently above threshold, then the departure due to the difference in slope becomes very obvious. These measurements made are within the constraints of the linear operating region above threshold on the *LI*-curve, this parameter thus needs to be computed as point slope in the event of effects such as spatial hole burning or tendency of the gain to reach saturation

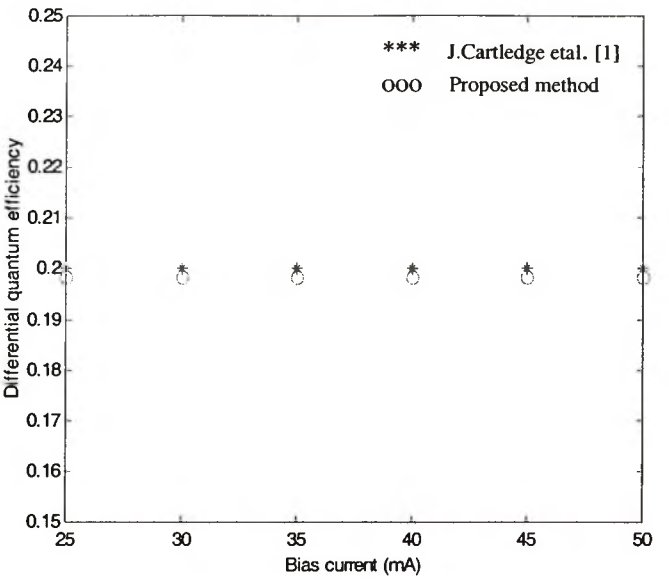

Fig.5.6 External slope efficiency in comparison with the reported values in [1]. The values remain the same throughout the linear operating region above threshold

The biggest difference amongst corresponding parameters is observed for the photon lifetime (figure-5.7), the computed values are around 1.5ps whereas the optimized values from [1] are less than 1ps. The latter would imply a cavity length which is physically very difficult to achieve in terms of fabrication, at higher bias levels however, this value approaches 2ps.

The increase in photon lifetime with bias current is consistent with the device physical behavior, where the lifetime is very high below threshold but drops sharply as the laser reaches its threshold point. Above threshold, it increases only slightly with increasing input powers. Since the computed lifetime is dependent on the parameter '$\overline{a}$', the drift is caused by the changing value of this parameter given that the carrier lifetime

and threshold current in the relation, are both constant. Large signal analysis will show how the difference between the parameters affects the response curve.

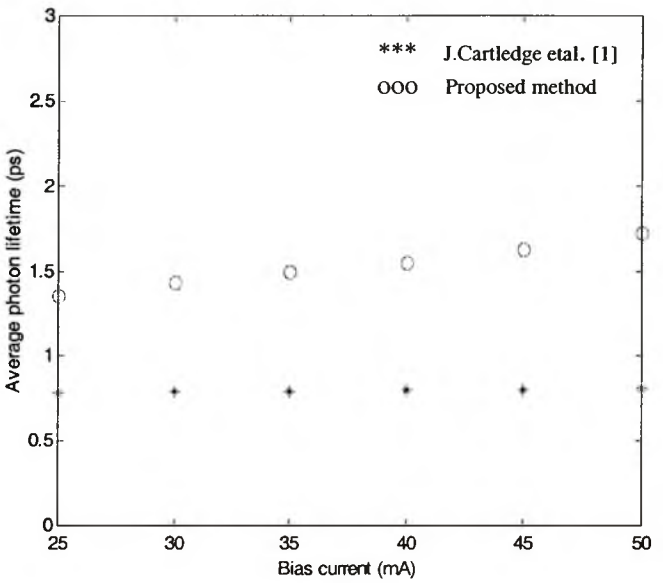

Fig.5.7 The computed values of photon lifetime are nearly twice that of those reported in [1] with a higher degree of change with increasing bias

Once the photon lifetime is determined, the K-factor from the small signal response would yield parameter '$\bar{b}$' which remains nearly uniform at all bias levels (figure-5.8). Note that at low injection levels, the reported value of this parameter from [1] is slightly higher than the computed value from the proposed method, but it soon adjusts to this value for higher injection currents.

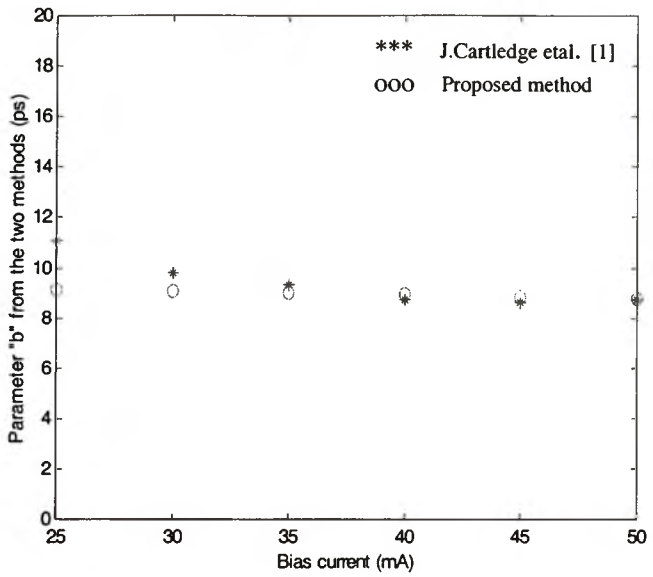

Fig.5.8 The optimized solution for the parameter from [1] adjusts to the values estimated using our proposed method at higher bias

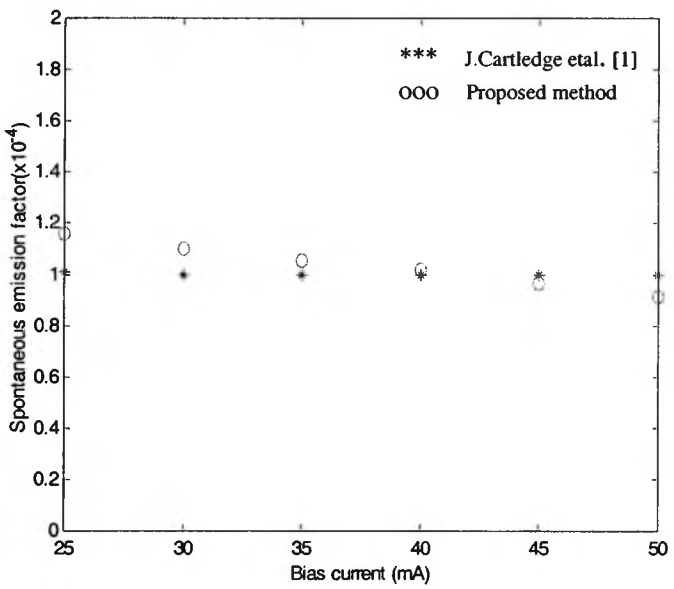

Fig 5.9 A comparison between the corresponding values of spontaneous emission factor from the two methods

Figure-5.9 shows the comparison for the spontaneous emission-coupling factor. We would expect the computed value to change sharply with higher bias, due to the large drift in the average photon lifetime; however, we observe only a slight decrease in value and very close to the reported value at all injection levels.

The analysis in extracted parameter values from the two methods show expected differences, some greater than others, but the important conclusion that can be drawn from this is that there is a certain degree of correlation between the computed values from the two procedures. Irrespective of the individual differences, the unique combination of parameters from both methods within the rate equation model should be able to produce comparable results for large signal response in order to lend credibility to the effectiveness of our proposed methodology.

5.3.3 Comparison of large signal response simulations

For the above threshold condition, first the laser is pre-biased at 35mA and a dc input current of 10mA is applied over and above the initial bias to observe response to the small step input. The parameters were computed at the bias current of 35mA.

The simulated behavior compares well with that obtained from using the reported parameter values of [1]. Carrier lifetime estimates only slightly affect the response (figures-5.10 and 5.11). The difference becomes even more insignificant as the laser is driven strongly to higher bias levels as shown in figure-5.12. Here the laser is pre-biased very close to threshold (20mA), not withstanding mounting fixture noise affects, and subjecting the device to a dc input of 45mA over and above the initial bias. The simulation results from the two methods are quite identical.

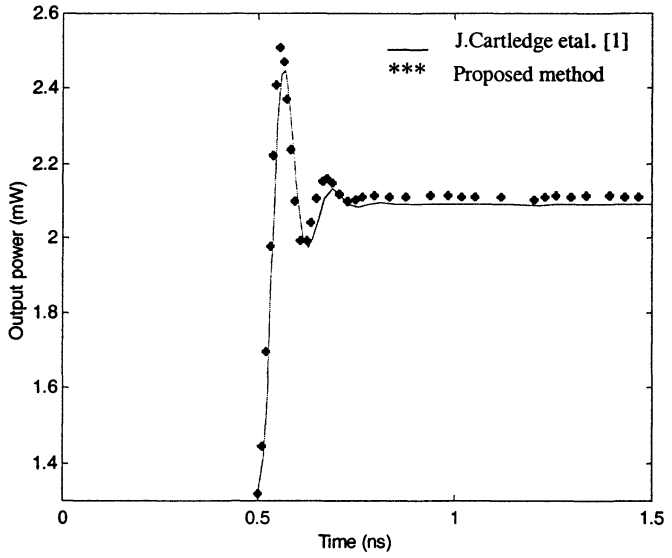

Fig.5.10 Response to a step input current pulse of 35-45mA, with differential carrier lifetime as modal parameter

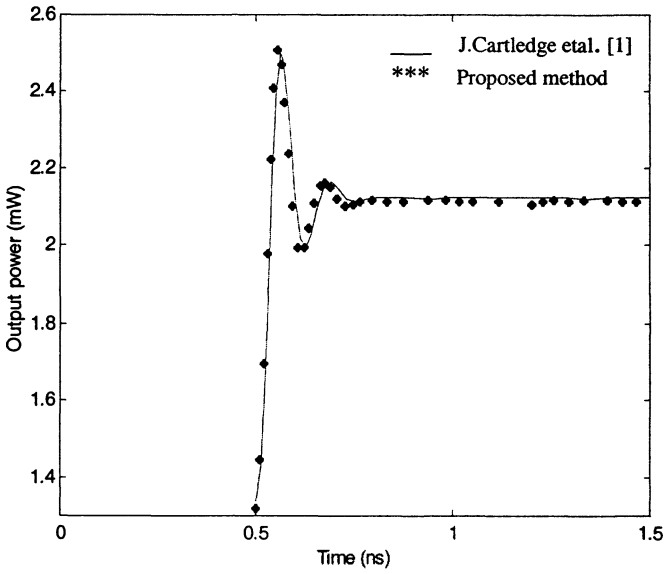

Fig.5.11 Response to a step input current pulse of 35-45mA, with total carrier lifetime as modal parameter

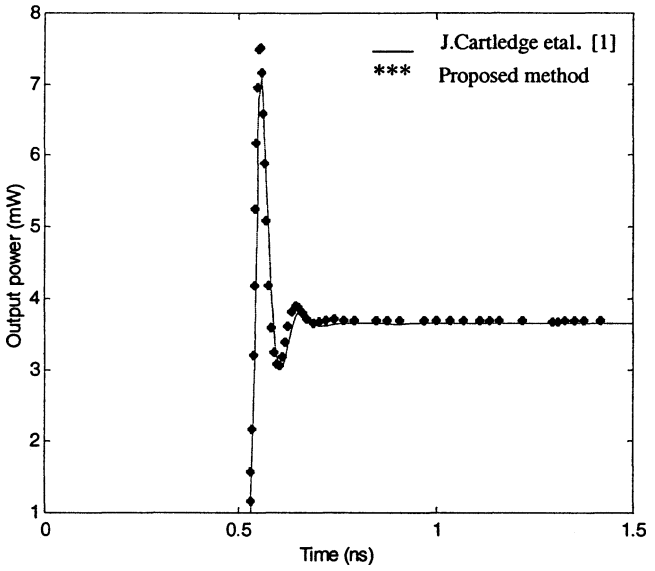

Fig.5.12 Response to a step input current pulse of 20-65mA, with differential carrier lifetime as modal parameter

The comparison in frequency chirp from the two methods at 35mA show somewhat dissimilar results, but the absolute difference in frequency is within 1GHz. For a strongly driven case the results are much more identical. (Figure-5.13). The parameter of linewidth enhancement factor is obtained from the results presented in [1].

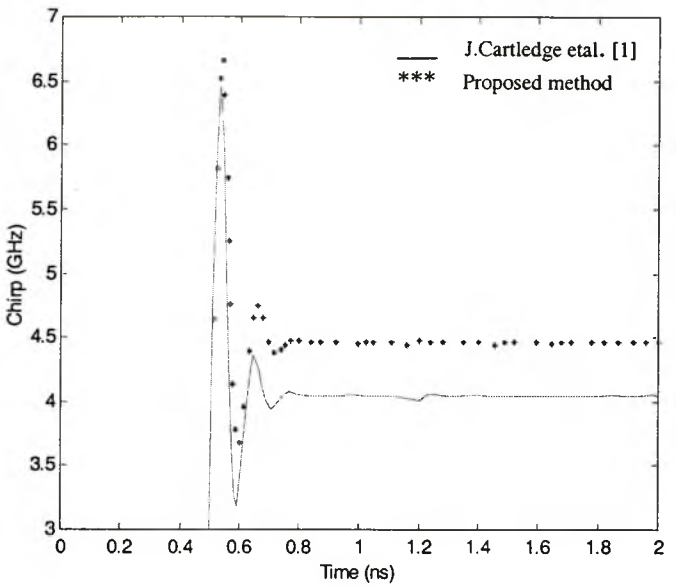

(a)

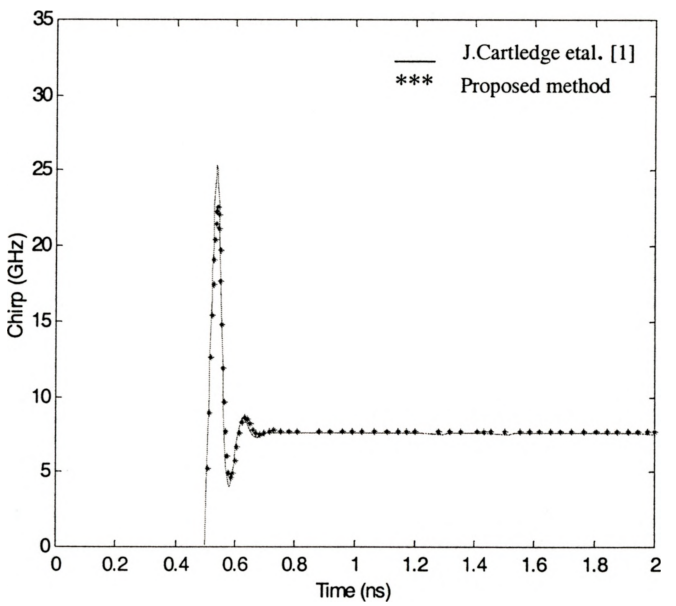

(b)

Fig.5.13 Comparison of frequency chirp from the two methods due to a step input bias (a) 35mA to 45mA (b) 20mA to 65mA

The steady-state *LI-* curve points obtained from the large signal simulations are compared with the measured output power at different bias points as shown in figure-5.14, observe the very slight difference at higher bias due to the small difference in slope.

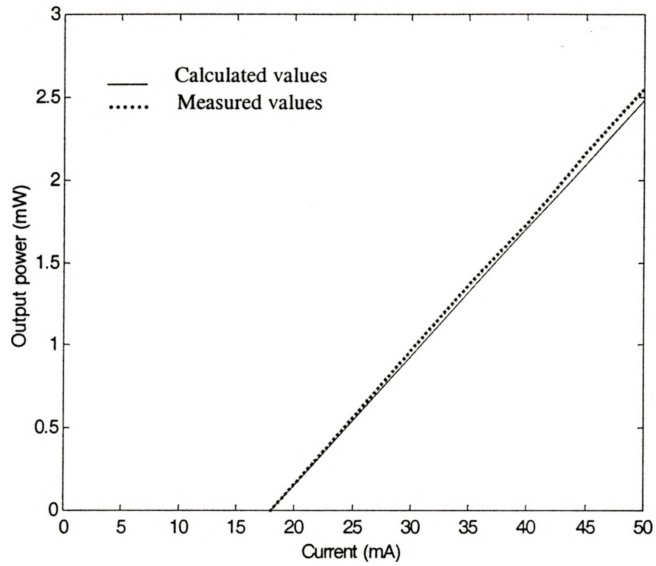

Fig.5.14 Measured output power above threshold compared with computed values from large signal analysis at different bias levels

5.3.5 Test for robustness

To test our model for robustness in terms of the range of parameters over which the output response would be good, we can vary each parameter individually and then observe the affect on the behavior. But this may not be a realistic approach. The reason being that our procedure is entirely analytical in nature and there are no 'initial estimates', all the computed parameters are linked to one another through well-defined

functional relationships; thus, causing a change in the value of one parameter would invariably cause a change in the others.

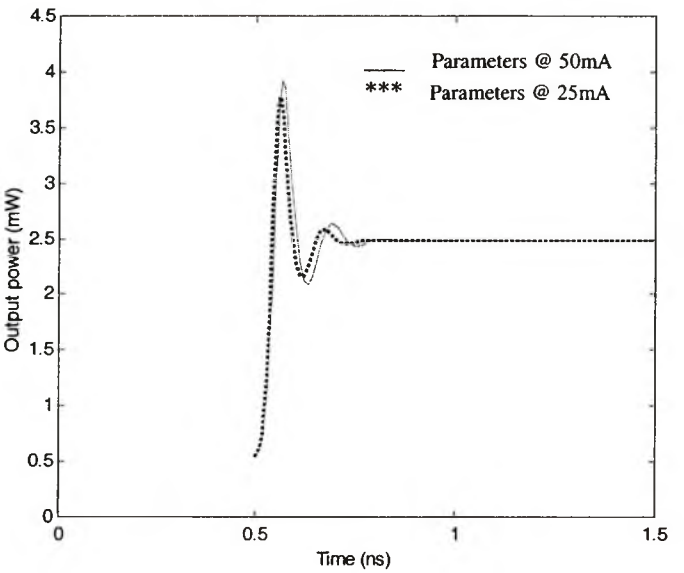

Fig.5.15 Step response to an input of 20-50mA but with parameters computed at 25mA bias and 50mA bias currents respectively

We have observed in the preceding comparisons that there is sufficiently significant variation in the parameter values over the entire range of laser bias current levels. Thus the best way to test the method would be to check the response at one extreme end of the bias point using the parameters computed at the other extreme end of bias or vice versa.

We bias the laser close to threshold (20mA) and apply a step input of 30mA over and above this level, but with one exception. The response at two parameter sets is from

different bias levels but come from the same extraction process. In the first step, the parameters computed at a bias current of 25mA are used and the response generated. In the second step, the parameters computed at 50mA are used and the response is generated. A comparison is shown in figure-5.15.

At higher bias levels, the parameters produce a stronger 'ring' in the response as well as a slight drift in resonance frequency, which tends to decrease. Other than this, the two functions are similar. It is important to note that the variation observed here is for the worst-case scenario, the parameters for a particular bias point can be extrapolated from the computed parameters at some other bias levels and would fall within the acceptable limits since the drift in parameters would follow a more or less linear path.

5.4 Comparisons in 'Laser-B'

In the second example, we only use "measured" values above threshold within a small range of bias currents and for higher values of injected current we extrapolate to obtain parameters. Backward extrapolation was limited due to unstable results of small signal parameter measurements close to threshold.

The measured and calculated values of damping coefficient show good conformance in the selected bias range (Figure-5.16). The measured small signal parameters and the corresponding computed rate equation parameters are listed in table-5.4 and table-5.5 respectively.

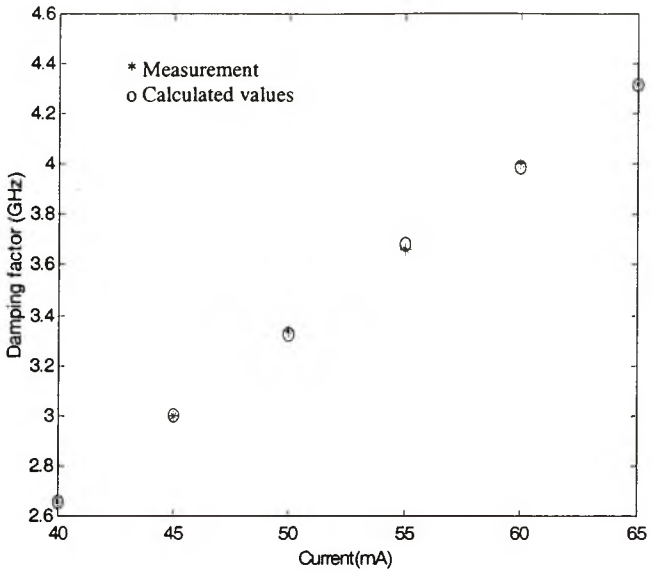

Fig.5.16 Comparison of measured (ALDS simulation) and calculated values of the damping factor (small signal parameter)

Parameters	**Bias current (mA)**					
	40	**45**	**50**	**55**	**60**	**65**
$P_1(mW)$	2.5	3.3	4.16	5.0	5.83	6.67
$Y_1(x10^9\ \mathrm{sec}^{-1})$	2.66	3.0	3.34	3.66	4.0	4.32
$\omega_0^2(x10^{20}\ Hz^2)$	7.64	9.87	11.94	14.21	16.17	18.25

Table 5.4

Parameters	Bias Current (mA)					
	40	**45**	**50**	**55**	**60**	**65**
$\bar{a}(GHz^2/mA)$	47.2	46.5	45.6	45.5	44.7	44.3
$\bar{b}(x10^{-12}s)$	0.026	0.025	0.022	0.022	0.019	0.018
$\bar{c}(A/W)$	6.41	6.41	6.41	6.41	6.41	6.41
$\tau_P(x10^{-12}s)$	1.3	1.32	1.35	1.35	1.374	1.385
$\tau_N(x10^{-9}s)$	1.37	1.37	1.37	1.37	1.37	1.37
$\beta(x10^{-4})$	0.434	0.428	0.418	0.418	0.41	0.407
$I_{TH}(x10^{-3}A)$	23.8	23.8	23.8	23.8	23.8	23.8
$P_1(x10^{-3}W)$	2.5	3.3	4.16	5.0	5.83	6.67

Table 5.5

For large signal simulations, the laser was pre-biased at 25mA (only slightly above the threshold value) and step inputs of 25mA and 75mA were applied over and above the bias point, to observe behavior. A strong resonance and comparatively weak damping is predictably expected in both cases.

The simulation and measured results compare very favorably in the first case (25mA step input), however the more complex ALDS model seems to depict a relaxation in the resonance with the passage of time which is not observed for our simple 0D- rate equation model (figure-5.17).

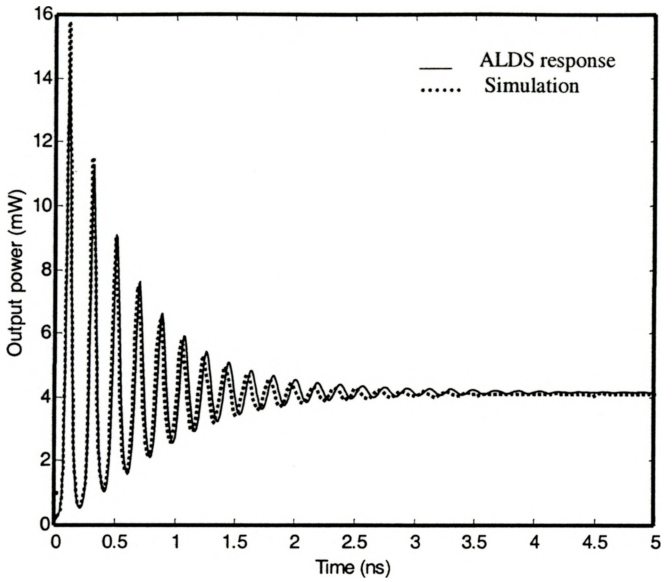

Fig.5.17 Measured (ALDS simulated) and computed response to step input from 25mA to 50mA

This may be attributed to the fact that no structural parameters are included in the model and as a result no spatial phenomenon can be accounted for which might be available from the ALDS simulator. This shows one particular drawback of using a simpler model.

In the second case (75mA step input), the output was found to be slightly less then the measured response due to change in slope of the LI-curve attributed to spatial hole burning (figure-5.18(b)). Since the initial parameter set (measured at 50mA) is used to generate response, change in slope is not reflected by the output, which explains the disparity in results shown in figure-5.18(a).

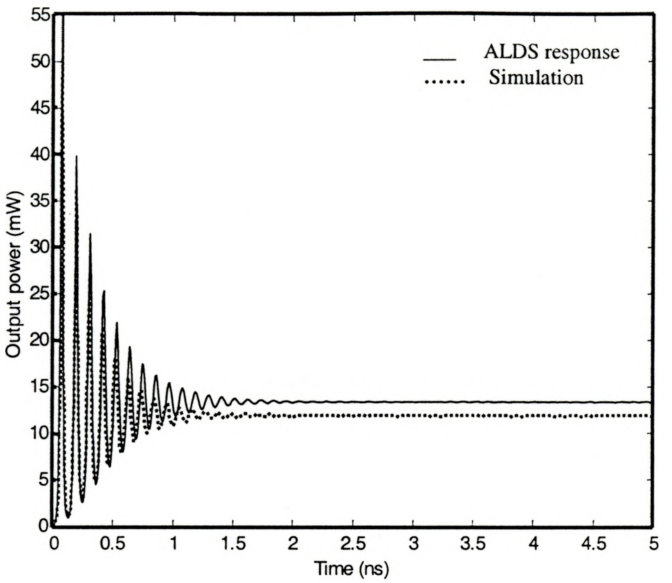

(a)

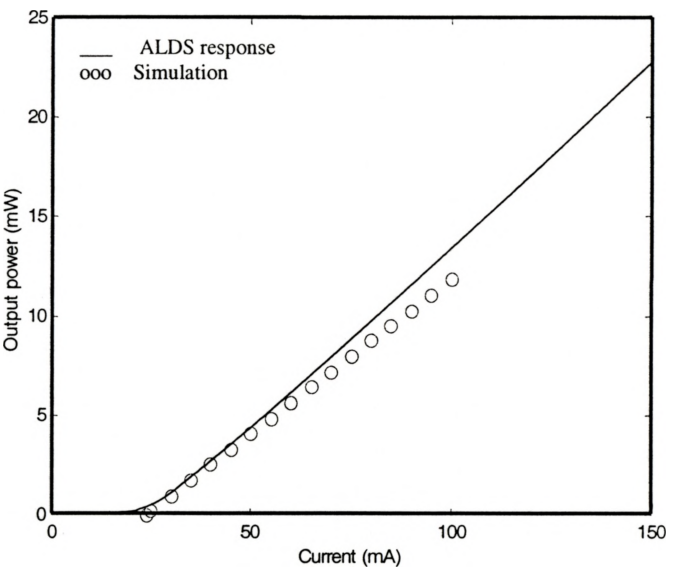

(b)

Fig.5.18 (a) Difference in output (bias from 25mA to 100mA) due to change in slope (b) Measured and computed LI-curves using the parameters measured at 50mA. Observe the difference in slope at higher bias levels

If the parameters are computed at the maximum bias level obtained from the referencing input signal then any changes in slope will be automatically taken into account by the computed parameter $\bar{c}$, measured at that injection level, as the information will be available from the *LI*-curves as long as it is within the available measurement range. In this case though, by adjusting the parameter $\bar{c}$ slightly above its computed value (slope increased from 0.417 to 0.47) to approximate the measured power, we are able to match the results from the ALDS simulator as shown in figure-5.19, again, without using any optimization routine. The relaxation of the resonant frequency with time is still present as in the previous case, but the results are accurate enough to account for the greater part of the response variations.

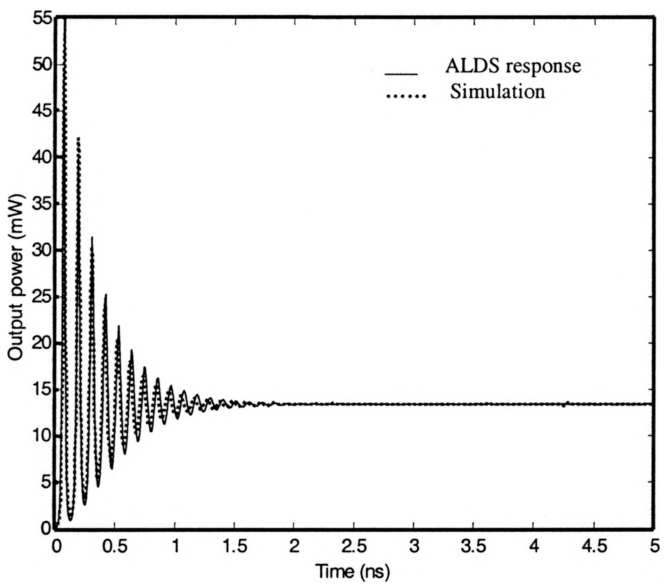

Fig.5.19 Comparison of simulated response and ALDS generated output to a step input of 25mA-100mA for parameter set computed at 100mA bias

5.4.1 Analysis for below-threshold bias

In chapter-4, we have proposed a simple method of predicting response of below-threshold biased lasers, by modifying only two of the modal parameters. We estimate the total carrier lifetime based on the assumption that only bimolecular recombination is of significance close to threshold, as it also defines the spontaneous emission coupling in the mode of interest. With negligible auger and non-radiative recombination effects, the carrier lifetime simply becomes

$$\tau_N \approx 2\tau_{\Delta N}$$

Similarly, the spontaneous emission factor is a fraction multiple of the estimated value at threshold assuming this to provide the average contribution to the lasing mode below threshold. Since the turn-on delay for laser with below-threshold bias is directly related to the absolute change in the carrier density which in-turn is defined by the total carrier lifetime, we should be able to predict the governing large signal response if our estimate for the lifetime and the below-threshold spontaneous emission contribution is accurate enough.

For laser-B, in order to test for turn-on delay estimations we again generate a step input response from the ALDS for both 50mA and 100mA biases as was the case earlier, but this time, we have zero initial bias before the application of input, thus the generated response for the quarter-wave shifted DFB (simulated) laser includes the maximum turn-on delay. A comparison of the ALDS generated response with our model is shown in figure-4.20. The comparison in response is much improved from that reported in [2]. A slight difference in turn-on delay is observed as would be expected as a result of the approximations made.

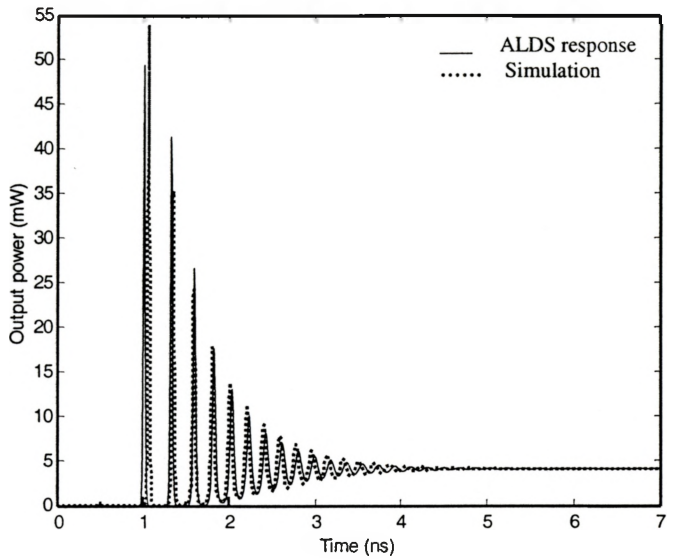

(a)

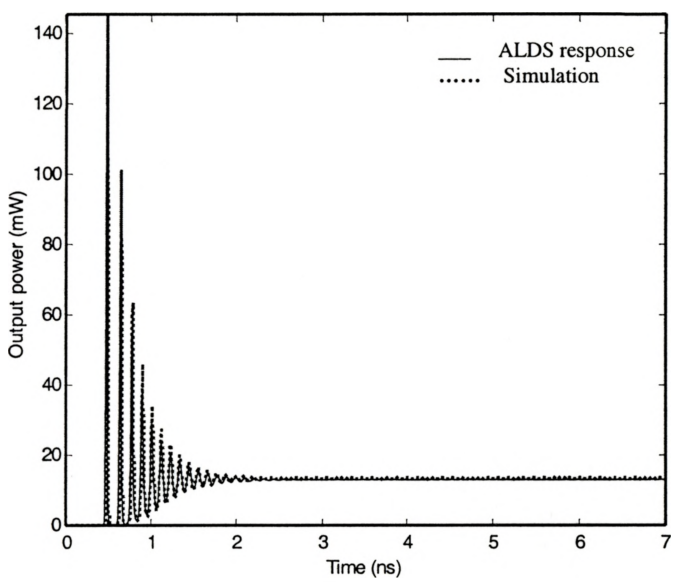

(b)

Fig.5.20 Computed response (a) at 50mA and (b) at 100mA, from zero initial bias showing the comparison of maximum turn-on delay and the peak transient

Here, we have shown that the 0D rate equation behavior model can be used to predict the effects of below threshold dynamics of the laser, if we can accurately predict the spontaneous emission contributions below threshold and the total carrier lifetime, these two parameters alone would be sufficient to account for the turn-on delay and the above threshold transients in the response, which have previously been un-accounted for ([1], [2]) in the rate-equation models.

Chapter-6

Conclusion

In this thesis we have presented a new method of parameter extraction from the 0D rate equation behavior model of a single mode semiconductor diode laser. The model itself has been modified to reduce the total number of extractable unknowns. Some of the parameters have been combined to represent a new set of measurable quantities. The transformation allows us to use only steady state *LI*-characteristics and the small signal parameters of resonant frequency and damping coefficient as inputs to completely characterize the large signal behavior.

The approach used in this work is similar to the one presented in [2], however, the proposed method is found superior in its ability to rely solely on the measured data of the DUT without requiring information of the frequency spectrum or the dispersion through a coupled fiber. Additionally, all the parameters are shown to be estimated only from above threshold measurements. In comparison with the numerical optimization method presented in [1], the proposed method has lesser degree of freedom with the estimations but does not suffer from the problems of initial value sensitivity or long computation time. Comparisons of the large signal response have shown that results from both methods are nearly identical in behavior despite the obvious differences in the computed parameters.

There are a couple of firsts in our work. We have for the first time, proposed a method to predict the spontaneous emission coupling factor into the lasing mode, only from above-threshold analysis. We have also correlated the behavior of a below-threshold biased quarter-wave shifted DFB laser directly to the modal parameters of spontaneous emission factor and carrier lifetime, where the latter is estimated from the small signal response alone. We have for the first time shown that a 0D behavior model can be used to predict turn-on delay and transients under the given bias conditions.

We have for the first time presented a complete thermal model of the edge-emitter laser, based on the proposed modified rate equation model, which encompasses all the thermal effects but requires only threshold current characteristic temperature as additional data which is readily available from the *LI*-characteristics.

In summary, a complete behavioral model has been investigated which shows to require less device data as input, is as accurate as its more complex counterparts, very fast in execution and covers all aspects of possible operating conditions.

6.1 Future research direction

This thesis has shown that a simple 0D model can go a long way towards comprehensive characterization of semiconductor lasers. This needs to be extended to include extraneous affects on the behavior such as noise and jitters. Moving away from the single mode operation, multimode lasers might be considered as possible candidates for modeling using a similar approach. Although, the proposed method is shown to be accurate, we cannot ignore the spatial affects inside the cavity, which affect the behavior. There is thus a need to use this approach in correlation with high-level models to develop a more representative model but with less complexity.

Bibliography

[1] John C. Cartledge, R.C. Srinivasan, "Extraction of DFB Laser Rate Equation Parameters for System Simulation Purposes", *J. Lightwave Technol.*, vol.15, pp.852-860. May 1997.

[2] Leif Bjerken, Arne Royset, Lars Hafskjaer, Dagfinn Myhre, "Measurement of Laser Parameters for Simulation of High-Speed Fiber Optic Systems", *J. Lightwave Technol.*, vol.14, pp.839-850. May 1996.

[3] L.A.Coldren, S.W.Corzine, *Diode Lasers and Photonic Integrated Circuits,* New York: Wiley c1995. pp. 1-594.

[4] X.Li, A.D.Sadovnikov, W.P.Huang, T.Makino, "A Physics-Based Three-Dimensional Model for Distributed Feedback Laser Diodes", *IEEE J. Quantum Electron.* , vol.34, pp. 1545-1553, Sepetember 1998.

[5] P.V.Mena, J.J.Morikuni, S.M.Kang, A.V.Harton, K.W.Wyatt, "A Simple Rate-Equation-Based Thermal VCSEL Model", *J. Lightwave Technol.*, vol.17, pp. 865-872, May 1999.

[6] K.Czotscher, S.Weisser, A.Leven, J. Rosenweig, " Intensity Modulation and Chirp of 1.55 μm Multiple Quantum Well Laser Diodes: Modeling and Experimental Verification", *IEEE J. Select. Topics Quantum Electron.*, vol.5, pp. 606-612, May/June 1999.

[7] P.A.Morton, T.Tanbun-Ek, R.A.Logan, A. M. Sergent, P.F.Sciortino Jr., D.L.Coblentz, " Frequency Response Subtraction for Simple Measurement of

[8] Rodney S. Tucker, "Large-signal circuit model for simulation of injection-laser modulation dynamics", *IEE Proc.,* vol.128, Pt.1, pp. 180-184, October 1981.

[9] R.Paoletti, M.Meliga, I.Montrosset, "Optical Modulation Technique for Carrier Lifetime Measurement in Semiconductor Lasers", *IEEE Photon. Technol. Lett.* , vol.8, pp. 1447-1449, November 1996.

[10] J.E.Bowers, "High Speed Semiconductor Laser Design and Performance", *Solid State Electron.,* vol.30, pp. 1-11, 1987.

[11] X.Li, Wie-Ping Huang, "Simulation of DFB Semiconductor Lasers Incorporating Thermal Effects", *IEEE J. Quantum Electron.,* vol.31, pp. 1848-1855, October 1995.

[12] D.F.Zaitsev, "Temperature Drift of Modulation Characteristics in Semiconductor Lasers", *IEE Proceedings-J.* Vol. 140, No.4, August 1993.

[13] Pankov, J.I, "Temperature dependence of emission efficiency and lasing threshold in laser diode.", *IEEE J. Quantum Electron.*, vol.4, pp 119-122, 1968.

[14] A.A.Saavedra, R.Passy, J.P.Vod der Weid, "Thermal drift in wavelength switching DFB and DBR lasers", *Electron. Lett.,* vol.33, pp. 780-781, 1997.

[15] K.Y.Lau, A.Yariv, "Ultra-high speed semiconductor lasers" , *IEEE J. Quantum Elecrton.,* vol.21, pp.121-138, 1985.

[16] S.Kobayashi, Y.Yamamoto, M.Ito, T.Kimura, "Direct frequency modulation in AlGaAs semiconductor lasers", *IEEE J. Quantum Electron.,* vol. 18, pp.582-595, 1982.

[17] J.Wang, K.Petermann, "Small signal analysis for dispersive optical fiber communication systems", *J. Lightwave Technol.,* vol.10, pp.96-100, 1992.

[18] L.M.Zhang, J.E.Carrroll, "Large-signal dynamic model of the DFB laser", *IEEE J. Quantum Electron.,* vol. 28, pp.604-611, 1992.

[19] J.Hong, Wie-Ping Huang, T.Makino, "Static and dynamic simulations for ridge-waveguide MQW DFB lasers", *IEEE J. Quantum Electron.,* vol.31, pp.49-59, 1995.

Appendix - A

Derivation for the 'Modified' Rate Equation Model

Reproducing the rate equations from the 'universal' time domain model

$$\frac{dS}{dt} = \frac{\Gamma g_0 (N - N_T) S}{(1 + \varepsilon S)} - \frac{S}{\tau_P} + \Gamma \beta \frac{N}{\tau_N} \tag{A-1}$$

$$\frac{dN}{dt} = \frac{I}{qV} - \frac{g_0 (N - N_T) S}{(1 + \varepsilon S)} - \frac{N}{\tau_N} \tag{A-2}$$

$$\frac{d\phi}{dt} = \alpha \frac{1}{2} \Gamma g_0 (N - N_{th}) \tag{A-3}$$

Solving for equation (A-1), we multiply and divide the first term on the RHS by qV

$$\frac{dS}{dt} = \frac{\frac{\Gamma g_0}{qV} (N - N_T) qVS}{(1 + \varepsilon S)} - \frac{S}{\tau_P} + \Gamma \beta \frac{N}{\tau_N} \tag{A-4}$$

Under steady state conditions neglecting all space dependent effects, we can approximate

$$\Gamma g_0 (N_0 - N_T) \approx \frac{1}{\tau_P}$$

$$\therefore N_T = N_0 - \frac{1}{\Gamma g_0 \tau_P}$$

$$N_T V = N_0 V - \frac{V}{\Gamma g_0 \tau_P \tau_N}$$

Multiply and divide the first term on RHS by τ_N

$$N_T V = \frac{N_0 V \tau_N}{\tau_N} - \frac{V}{\Gamma g_0 \tau_P \tau_N} \tag{A-5}$$

At threshold current, the following relationship holds

$$\frac{N_0}{\tau_N} = \frac{I_{TH}}{qV}$$

Therefore, expressing in terms of threshold current in (A-5)

$$N_T V = \frac{I_{TH} V \tau_N}{qV} - \frac{V}{\Gamma g_0 \tau_P \tau_N}$$

$$N_T V = \frac{I_{TH} \tau_N}{q} - \frac{qV}{\Gamma g_0 \tau_P \tau_N q}$$

Making the appropriate substitutions in equation (A-4), from above, we have

$$\frac{dS}{dt} = \frac{\frac{\Gamma g_0}{qV}\left(qNV - \left(I_{TH}\tau_N - \frac{qV}{\Gamma g_0 \tau_P \tau_N}\right)\right)S}{(1+\varepsilon S)} - \frac{S}{\tau_P} + \Gamma\beta\frac{N}{\tau_N} \tag{A-6}$$

Photon density from one facet of a single facet HR-coated device can be expressed in terms of output power by the following relationship

$$S(t) = \frac{2\Gamma\tau_P}{V\eta_D h\upsilon} P(t) \tag{A-7}$$

Replacing $S(t)$ with the above relation in (A-6) (except the gain compression term in the denominator), we have

$$\frac{d}{dt}\left(\frac{2\Gamma\tau_P P}{V\eta_D h\upsilon}\right) = \frac{\frac{\Gamma g_0}{qV}\left(qNV - I_{TH}\tau_N + \frac{qV}{\Gamma g_0 \tau_P \tau_N}\right)\left(\frac{2\Gamma\tau_P P}{V\eta_D h\upsilon}\right)}{(1+\varepsilon S)} - \frac{2\Gamma\tau_P P}{V\eta_D h\upsilon\tau_P} + \Gamma\beta\frac{N}{\tau_N}$$

$$\left(\frac{2\Gamma\tau_P}{V\eta_D h\upsilon}\right)\frac{dP}{dt} = \left(\frac{2\Gamma\tau_P P}{V\eta_D h\upsilon}\right)\frac{\frac{\Gamma g_0}{qV}\left(qNV - I_{TH}\tau_N + \frac{qV}{\Gamma g_0 \tau_P \tau_N}\right)}{(1+\varepsilon S)} - \frac{2\Gamma P}{V\eta_D h\upsilon} + \Gamma\beta\frac{N}{\tau_N}$$

After cross multiplication, we have

$$\frac{dP}{dt} = \left(\frac{\Gamma g_0 P}{qV}\right)\frac{\left(qNV - I_{TH}\tau_N + \frac{qV}{\Gamma g_0 \tau_P \tau_N}\right)}{(1+\varepsilon S)} - \frac{P}{\tau_P} + \beta NV\left(\frac{\eta_D h\upsilon}{2\tau_P\tau_N}\right)$$

$$\frac{dP}{dt} = \frac{\left(\frac{\Gamma g_0}{qV}\right)(qNV - I_{TH}\tau_N)}{(1+\varepsilon S)}P + \frac{P}{\tau_P(1+\varepsilon S)} - \frac{P}{\tau_P} + \beta NV\left(\frac{\eta_D h\upsilon}{2\tau_P\tau_N}\right)$$

$$\frac{dP}{dt} = \frac{\left(\frac{\Gamma g_0}{qV}\right)(q(NV) - I_{TH}\tau_N) + \frac{1}{\tau_P}}{(1+\varepsilon S)}P - \frac{P}{\tau_P} + \beta(NV)\left(\frac{\eta_D h\upsilon}{2\tau_P\tau_N}\right) \tag{A-8}$$

Solving for equation (A-2) in a similar manner, we multiply throughout by V

$$\frac{d}{dt}(NV)=\frac{I}{q}-\frac{g_0(N-N_T)VS}{(1+\varepsilon S)}-\frac{(NV)}{\tau_N}$$

Making the appropriate substitutions for steady-state approximations stated above

$$\frac{d}{dt}(NV)=\frac{I}{q}-\frac{g_0\left((NV)-\left(\frac{I_{TH}\tau_N}{q}-\frac{qV}{\Gamma g_0\tau_P\tau_N q}\right)\right)S}{(1+\varepsilon S)}-\frac{(NV)}{\tau_N}$$

Again representing photon number in terms of output power

$$\frac{d}{dt}(NV)=\frac{I}{q}-\frac{g_0\left((NV)-\frac{I_{TH}\tau_N}{q}+\frac{qV}{\Gamma g_0\tau_P\tau_N q}\right)\left(\frac{2\Gamma\tau_P P}{V\eta_D h\upsilon}\right)}{(1+\varepsilon S)}-\frac{(NV)}{\tau_N}$$

$$\frac{d}{dt}(NV)=\frac{I}{q}-\frac{\frac{\Gamma g_0 2q\tau_P}{qV\eta_D h\upsilon}\left((NV)-\frac{I_{TH}\tau_N}{q}\right)+\frac{2}{\eta_D h\upsilon}}{(1+\varepsilon S)}P-\frac{(NV)}{\tau_N} \qquad \text{(A-9)}$$

Multiplying both sides of equation (A-7) by "ε", we have

$$\varepsilon S=\frac{2\varepsilon\Gamma\tau_P}{V\eta_D h\upsilon}P$$

$$\varepsilon S=\frac{2\varepsilon\Gamma\tau_P}{V\eta_D h\upsilon}x\frac{qg_0}{qg_0}xP$$

$$\varepsilon S = \tau_P \frac{\varepsilon}{g_0} x \frac{\Gamma g_0}{qV} x \frac{2Pq}{\eta_D h\upsilon}$$

Thus, equations (A-8) and (A-9) can now be written as

$$\frac{dP}{dt} = \frac{\left(\frac{\Gamma g_0}{qV}\right)\left(q(NV) - I_{TH}\tau_N\right) + \frac{1}{\tau_P}}{\left(1 + \frac{\varepsilon \tau_P \Gamma g_0 2q}{g_0 qV \eta_D h\upsilon} P\right)} P - \frac{P}{\tau_P} + \beta(NV)\left(\frac{\eta_D h\upsilon}{2\tau_P \tau_N}\right)$$

$$\frac{d}{dt}(NV) = \frac{I}{q} - \frac{\frac{\Gamma g_0 2q\tau_P}{qV\eta_D h\upsilon}\left((NV) - \frac{I_{TH}\tau_N}{q}\right) + \frac{2}{\eta_D h\upsilon}}{\left(1 + \frac{\varepsilon \tau_P \Gamma g_0 2q}{g_0 qV \eta_D h\upsilon} P\right)} P - \frac{(NV)}{\tau_N}$$

Through a proper combination of the parameters in the modified rate equations above, we can rewrite our rate equation model in terms of lumped parameter set.

$$\frac{dP}{dt} = \frac{\bar{a}\left(q(NV) - I_{TH}\tau_N\right)P + \frac{P}{\tau_P}}{\left(1 + \bar{a}\bar{b}\bar{c}\tau_P P_0\right)} - \frac{P}{\tau_P} + \beta(NV)\left(\frac{q}{\bar{c}\tau_P \tau_N}\right) \qquad \text{(A-10)}$$

$$\frac{d}{dt}(NV) = \frac{I}{q} - \frac{\overline{ac}\tau_P\left((NV) - \frac{I_{TH}\tau_N}{q}\right) + \frac{\bar{c}}{q}}{\left(1 + \bar{a}\bar{b}\bar{c}\tau_P P\right)} P - \frac{(NV)}{\tau_N} \qquad \text{(A-11)}$$

Where $\bar{a} = \frac{\Gamma g_0}{qV}$; $\bar{b} = \frac{\varepsilon}{g_0}$; $\bar{c} = \frac{2q}{\eta_D h\upsilon}$

The other three remaining unknowns are "τ_P", "τ_N"and "β". Thus we have reduced the total number of unknown parameters in the rate equation, from 9 to 6. These parameters (or combination of parameters) are extractable from the steady state *L-I* characteristics and the small signal AM-response of the laser. The uncoupled phase rate equation (A-3) can also be modified to be represented in terms of the parameters defined above.

$$\frac{d\phi}{dt} = \alpha \frac{1}{2} \Gamma g_0 (N - N_{th})$$

Multiply and divide RHS of the equation by 'qV'

$$\frac{d\phi}{dt} = \alpha \frac{1}{2} \frac{\Gamma g_0}{qV} (q(NV) - qVN_{th})$$

$$\frac{d\phi}{dt} = \alpha \frac{1}{2} \frac{\Gamma g_0}{qV} \left(q(NV) - qV\tau_N \frac{N_{th}}{\tau_N} \right)$$

Expressing the carrier density at threshold in terms of threshold current

$$\frac{d\phi}{dt} = \alpha \frac{1}{2} \frac{\Gamma g_0}{qV} (q(NV) - \tau_N I_{th})$$

$$\frac{d\phi}{dt} = \alpha \frac{1}{2} \bar{a} [q(NV) - I_{th}\tau_N] \qquad \text{(A-12)}$$

Equation (A-12) gives the modified phase rate equation and can be used directly to determine the frequency chirp.

Appendix - B

Design constraints for optimum operating point on the gain curve

Semiconductor laser designs for optical communication applications are focused around minimizing laser current using the adjustable parameters of the cavity combined with the intrinsic properties of the material used. For many laser designs, the knee of the gain curve defines the constraint for optimum operation characteristics and the threshold gain is placed closed to this point on the curve.

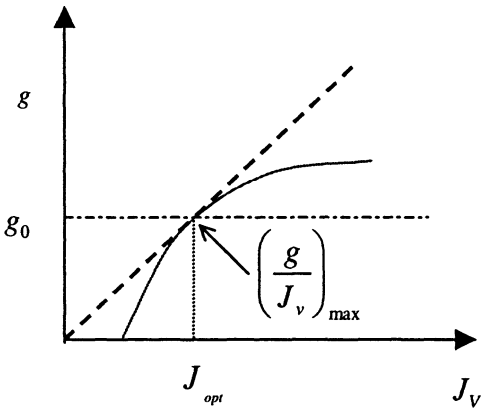

Fig.B1 Plot of material gain vs. volume current density

The following current density-gain equation shows this relationship

$$g = g_0 \ln\left(\frac{J + J_S}{J_T + J_S}\right) \quad \text{[Where "}J\text{" is the current density]}$$

If the linearity parameter (J_S) is zero (for positive gains), the solution is given by

$$J_{opt} = eJ_T \qquad \text{And} \qquad g_{opt} = g_0$$

$$\therefore \left(\frac{J_V}{g}\right)_{\min} = \frac{eJ_T}{g_0 L_z}$$

The width "L_z" is used because "J_V" is current per unit volume.

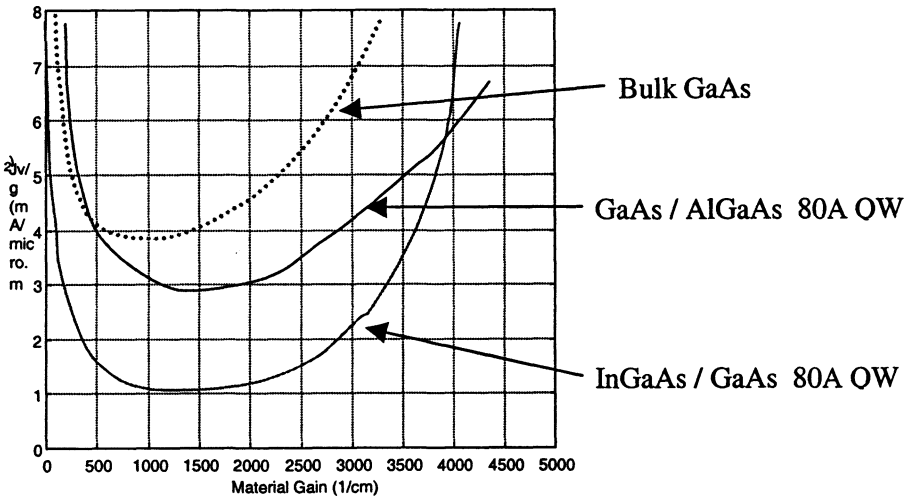

Fig.B2 Plot of calculated current-to-gain conversion factor as a function of material gain for three GaAs based active materials

The intrinsic gains of laser materials follow a typical profile with respect to the carrier density and in turn the input current. Figure-B2 is a plot of $\frac{J_V}{g}$ as a function of material gain for three *'GaAs'* based active materials which are the most commonly used material in semiconductor lasers. [3]

It can be observed from the above plots that as we move away on either side of the minimum of the curves, the value of the ratio $\frac{J_V}{g}$ increases significantly, indicating an increase in the threshold current. As we move to the right of this curve we are approaching smaller and smaller cavity lengths (which indicates smaller photon lifetime) and as we move away to the left of the minimum towards the transparency value, the cavity length increases (and so does the photon life time). It is clearly evident where the minimum $\frac{J_V}{g}$ occurs and how broad this minimum is, which can be summarized as follows

Active Materials	$\left(\frac{J_V}{g}\right)_{min}$	Material Gain
InGaAs QW	$1.4\ mA/\mu m^2$	$1250\,cm^{-1}$
GaAs QW	$2.9\,mA/\mu m^2$	$1450\,cm^{-1}$
Bulk GaAs	$3.8\,mA/\mu m^2$	$1000\,cm^{-1}$

Table B1

The graphs indicate that the penalty for operating too close to transparency is too high (in the form of very high threshold current). On the lower side of the gain the variation in slopes are nearly identical on all three materials.

Although the above values correspond to the lowest value of the ratio, the threshold gain can be selected anywhere within approximately 20% of this lowest value without too big a compromise on the threshold current.

For lasers that are designed for high speed applications, in addition to minimizing the laser current, we also want to maximize the differential gain in order to enhance the relaxation resonance frequency as indicated by the relation

$$\omega_0^{\,2} = \frac{g_0 S_0}{\tau_P}$$

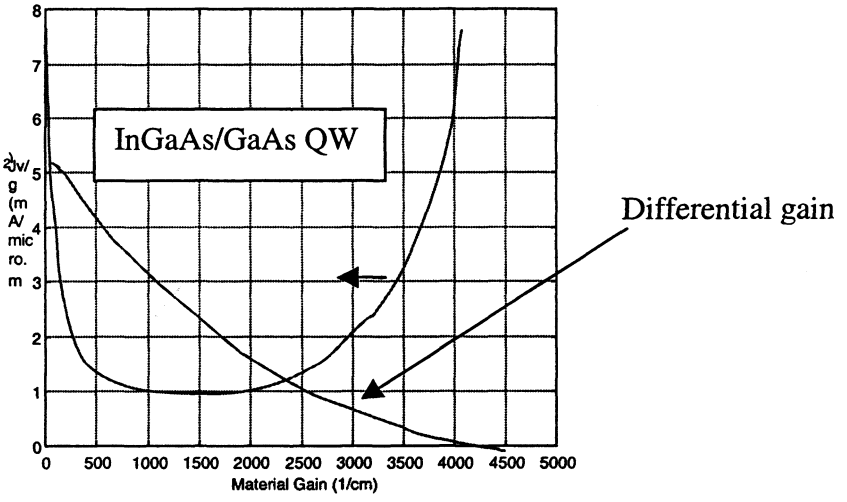

Fig.B3 Plot of current-to-gain conversion factor and differential gain as function of material gain for InGaAs/GaAs QW laser

However, the maximum differential gain occurs at transparency, which is far from ideal for minimizing the threshold current. Thus a trade off exists between obtaining low threshold current and high differential gain.

In the case of InGaAs/GaAs MQW laser, reducing the threshold material gain from $2000\,cm^{-1}$ to $1000\,cm^{-1}$ has little effect on the threshold current, while it increases the differential gain by nearly a factor of 2. Decreasing the material gain below $500\,cm^{-1}$ leads to large increase in threshold current without much increase in differential gain. Thus a reasonable compromise operating point exist somewhere in the range 500-$1000\,cm^{-1}$. This range lies at around 20% of the lowest value of J/g as described earlier. This constraint serves as a good figure of merit for estimation purposes.

Since the minimum point on the curve is well defined by the natural logarithmic function, and is nearly the same for all the device materials, we can approximate the optimum operating point for the high-speed laser by shifting towards the lower material gain within 20% of this minimum point on the curve. This will give us the best possible cavity length for the laser corresponding to the highest differential gain with lowest threshold current. Thus, irrespective of the type of material, an estimate can be made on the optimum value of photon lifetime without straying too far away from the actual value.

Also, it can be observed from the current-to-gain curves, that the lower bottom-left part of the curve for the three materials described above, are nearly identical, giving some credibility to the estimates for lasers made from these material. The gain relation is also described in terms of the carrier density by either an approximate linear relationship (which is used for most bulk lasers), or a more accurate logarithmic relationship.

$$g = g_0' \ln\left(\frac{N + N_S}{N_T + N_S}\right)$$

In this equation g_0' is an empirical gain coefficient and N_S is a shift to force the natural logarithm to be finite at $N = 0$, such that the gain equals the un-pumped absorption. However, if we limit ourselves to positive gains ($g \geq 0$), the above equation can be approximated as

$$g = g_0 \ln\left(\frac{N}{N_T}\right)$$

Where g_0 is the familiar differential gain coefficient.

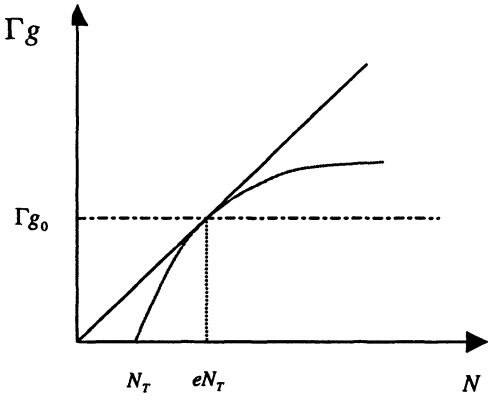

Fig.B4 Modal gain verses injected carrier density

Here the knee on the curve of carrier density corresponds to the minimum $\frac{J_V}{g}$ value described earlier.